1950

The effect of small holes on the stress distribution in webs subjected to pure bending

Karl, Richard Louis; Heller, Samuel R; Gerich, Walter R.

Massachusetts Institute of Technology

THE EFFECT OF SMALL HOLES ON THE STRESS DISTRIBUTION IN WEBS SUBJECTED TO PURE BENDING

RICHARD LOUIS KARL
SAMUEL RIES HELLER, JR.
WALTER RAYMOND GERICH

Cambridge, Massachusetts
May , 1950

Professor J. S. Newell
Secretary of the Faculty
Massachusetts Institute of Technology
Cambridge, Massachusetts

Dear Sir:

In accordance with the requirements for the degree of Naval Engineer we submit herewith a thesis entitled "The Effect of Small Holes on the Stress Distribution in Webs Subjected to Pure Bending".

Respectfully,

Richard L. Karl
Lieutenant Commander
U.S. Navy

Samuel R. Heller, Jr. [1920-]
Lieutenant
U.S. Navy

Walter R. Gerich
Lieutenant (junior grade)
U.S. Navy

THE EFFECT OF SMALL HOLES ON THE STRESS DISTRIBUTION IN WEBS SUBJECTED TO PURE BENDING

By

Richard Louis Karl,
Lieutenant Commander, U. S. Navy
B.S., U.S. Naval Academy, 1940

Samuel Ries Heller, Jr.
Lieutenant, U.S. Navy
B.S.E., University of Michigan
1941

Walter Raymond Gerich
Lieutenant (jg), U.S. Navy
B.S. U.S. Naval Academy, 1944

Submitted in partial fulfillment of the

requirements for the degree of

NAVAL ENGINEER

at the

MASSACHUSETTS INSTITUTE OF TECHNOLOGY
(1950)

Signature of Authors

_____

_____

_____
Department of Naval Arch. & Mar. Eng.
May , 1950

Certified by

_____
Thesis Supervisor

_____
Chairman, Departmental Committee on Graduate Students

ACKNOWLEDGEMENT

The authors wish to express their appreciation to those whose help was of such great value in the preparation of this thesis: to Professor W. M. Murray, W. L. Walsh, and G. H. Eisenhardt, of the Experimental Stress Analysis Laboratory who gave unstintingly of their time and effort to make the experimental work embodied in this report a success; to Professors C. H. Norris and J. H. Evans whose friendly advice and counsel served as a steady guide; to Professor R. D. Douglass for his assistance in checking the mathematics of the problem; to Professor J. P. den Hartog who proposed the study; and to Mr. J. S. Brock of the staff of the David Taylor Model Basin, Washington, D.C., for his pioneer work in the development of the theoretical solution and for his constant guidance at the inception.

TABLE OF CONTENTS

TABLE OF CONTENTS

SUMMARY

The object of this thesis is to determine the effect of small openings on the stress distribution in webs of beams subjected to pure bending and to devise a rapid means for predicting the increase in stress over that of the condition of no opening.

Experimental evidence for a family of specimens which covered the usual structural practice has been plotted in the RESULTS. A theoretical solution, developed in the APPENDIX, is included and compared with the experimental evidence. From these plots the authors conclude that: the theoretical solution compares quite favorably with actual experiment; the stress concentration factor for the edge of the hole varies directly with the ratio of depth of opening to depth of web and inversely with the ratio of length to depth of opening; and that the stress concentration factor for the edge of the web varies directly with the ratio of depth of opening to depth of web, but the variation with the ratio of length to depth of opening is more complex showing a pronounced maximum in the vicinity of 1.5. The fact that the ratio of depth of opening to depth of web is of little importance until it reaches the value of about 1/3 is considered excellent verification of presently accepted practice.

On the basis of the foregoing, it is considered highly desirable that further investigation for specimens having a ratio of length to depth of opening in the neighborhood of 1.5 be made with a view to confirmation. It is further considered desirable that a systematic survey of a similar

family be made to determine the effectiveness of reinforcement at openings and simultaneously cases of complex bending; i.e., bending with shear.

INTRODUCTION

In almost all structures openings of some sort are required, either for access of for passing piping, ventilation, or electrical systems to the various compartments. It, therefore, behooves the structural designer to make proper provision for these requirements without adversely affecting the structure.

Naturally, the circle, because of its simplicity, was the first type of opening chosen. Kirsch[1]* analyzed the effect of a circular opening in a uniform tension field; Tuzi[2] performed the analysis for the circular opening in pure bending; Howland and Stevenson[3] extended both the Kirsch and Tuzi analyses for finite width of plate and introduced the analysis for complex bending. Wolf[4] and Neuber[5] performed analyses for the elliptical opening in pure bending; Inglis[6] made a similar analysis for the elliptical hole in a uniform tension field; Wolf also extended his analysis to cover the ellipse in complex bending. Quite recently Greenspan[7] introduced an analysis for the flat ovaloid in a uniform tension field. In a forthcoming publication[8], Joseph and Brock develop a theoretical solution for the flat ovaloid in pure bending. This thesis is devoted to the latter problem. The theoretical solution in the APPENDIX follows the method proposed in (8). The effect of finite depth is evolved by an analysis of experimental data rather than by a rigorous mathematical method.

---

* Numbers in brackets refer to the Bibliography.

It is the purpose of this thesis to correlate data from photoelastic experiments with a systematic series of models with varying ratios of length to depth of opening and depth of opening to depth of web, subjected to pure bending, in which the openings are flat ovaloids; i.e., openings composed of rectangles with semicircles mounted at the longitudinal ends. This correlation includes a check on the mathematical solutions developed in (2), (3), (8), and in the APPENDIX.

PROCEDURE

The models were prepared using a nominal thickness of 3/8 inches clear Catalin. All models were cut from the same sheet of material, and a standard tensile specimen was included. The tensile specimen was used only to determine the fringe constant of the particular sheet to ensure satisfactory sensitivity as well as to provide means for obtaining checks through the equations of static equilibrium, if necessary. These models were machined using high-speed steel end mills for all cutting.

In an effort to minimize the time-edge effect, polymerization, a specimen was tested immediately after machining, allowing only sufficient time for machining stresses to dissipate. A white light polariscope was used for this purpose. The specimen was fitted with end brackets and suspended in an A - frame, as shown in Fig. I, which subjected the entire specimen to pure bending. Suspension was accomplished by vertical links fitted at each end with circular pins of drill stock to assure as nearly point support and loading as was feasible. The A - frame was located in the center of the circular polariscope using a mercury vapor lamp with a Wratten #62 Filter. The resulting light was very nearly monochromatic with a wave length of 5461 A°. The resulting fringes were alternately light and dark giving excellent contrast.

The specimen was first suspended with brackets and no load. The analyzer was rotated to give a dark field. A picture was taken in this condition, hereinafter referred to as "no load". The negative was then developed to assure proper focus before load was applied.

FIG. 1

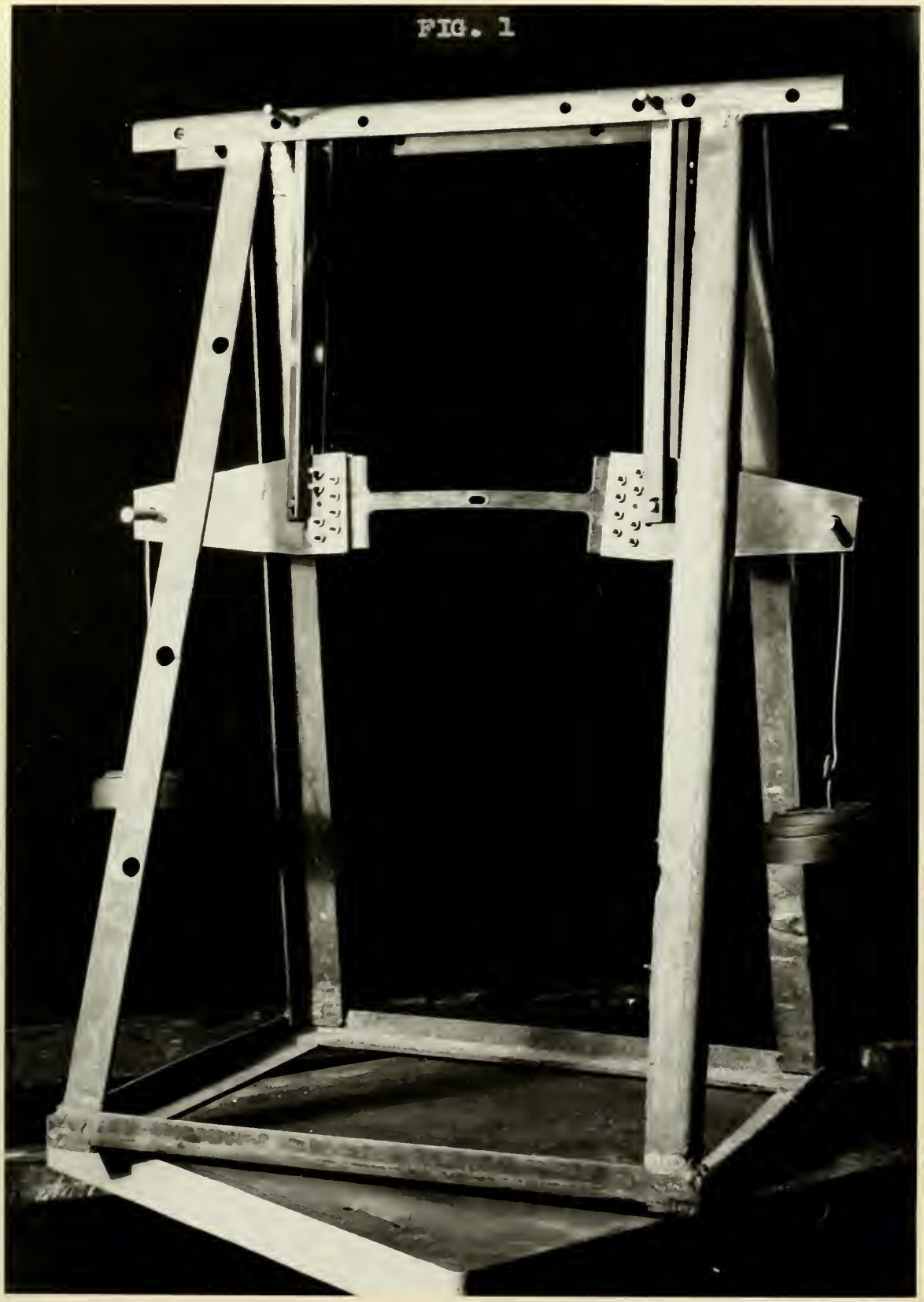

Load was then applied, and a new picture taken. The load was previously determined which would give a maximum stress of approximately 100 psi., well within the elastic range yet sufficiently high to give about seven (7) fringes. The analyzer remained in the same position as in the no load condition. The negative was then developed to assure satisfactory focus and contrast before the specimen was removed for further machining. By following this method, it was possible to complete a run, five (5) specimens - all with the same ratio of length to depth of opening, but with varying ratios of depth of opening to depth of web, in about four (4) hours which minimized the time-edge effect.

RESULTS

The results of the experimental data are incorporated in Figures II, III, IV, and V. Figure III is a plot of stress concentration factor at edge of hole versus the ratio of length to depth of opening for contours of depth of opening to depth of web. Figure II is a plot of stress concentration factor at the edge of the hole versus the ratio of depth of hole to depth of web for contours of constant ratios of length to depth of opening. On this plot the various experimental data is shown. Similarly Figure IV and V show respectively the same plots with stress concentration factor at the edge of web as the substituted variable. Table I is a compilation of experimental data from which the aforementioned curves have been plotted.

TABLE I

Summary of experimental data obtained photoelastically

Ratio of length to depth of opening	Ratio of depth of opening to depth of beam	Stress Concentration Factor	
a/b	b/c	Edge of hole	Edge of beam
	0.1115	2.067	1.060
	0.239	2.027	1.033
1.0	0.364	2.060	1.024
	0.485	2.180	1.040
	0.600	- - -	1.100
	0.100	1.430	1.045
	0.200	1.440	1.016
1.5	0.300	1.520	1.045
	0.400	1.648	1.124
	0.500	1.910	- - -
	0.100	1.320	1.026
	0.200	1.322	1.035
2.0	0.300	1.320	1.012
	0.400	1.410	1.072
	0.500	1.672	1.162
	0.100	1.160	1.077
	0.200	1.176	1.026
2.5	0.300	1.300	1.054
	0.400	1.280	1.087
	0.500	1.235	1.138

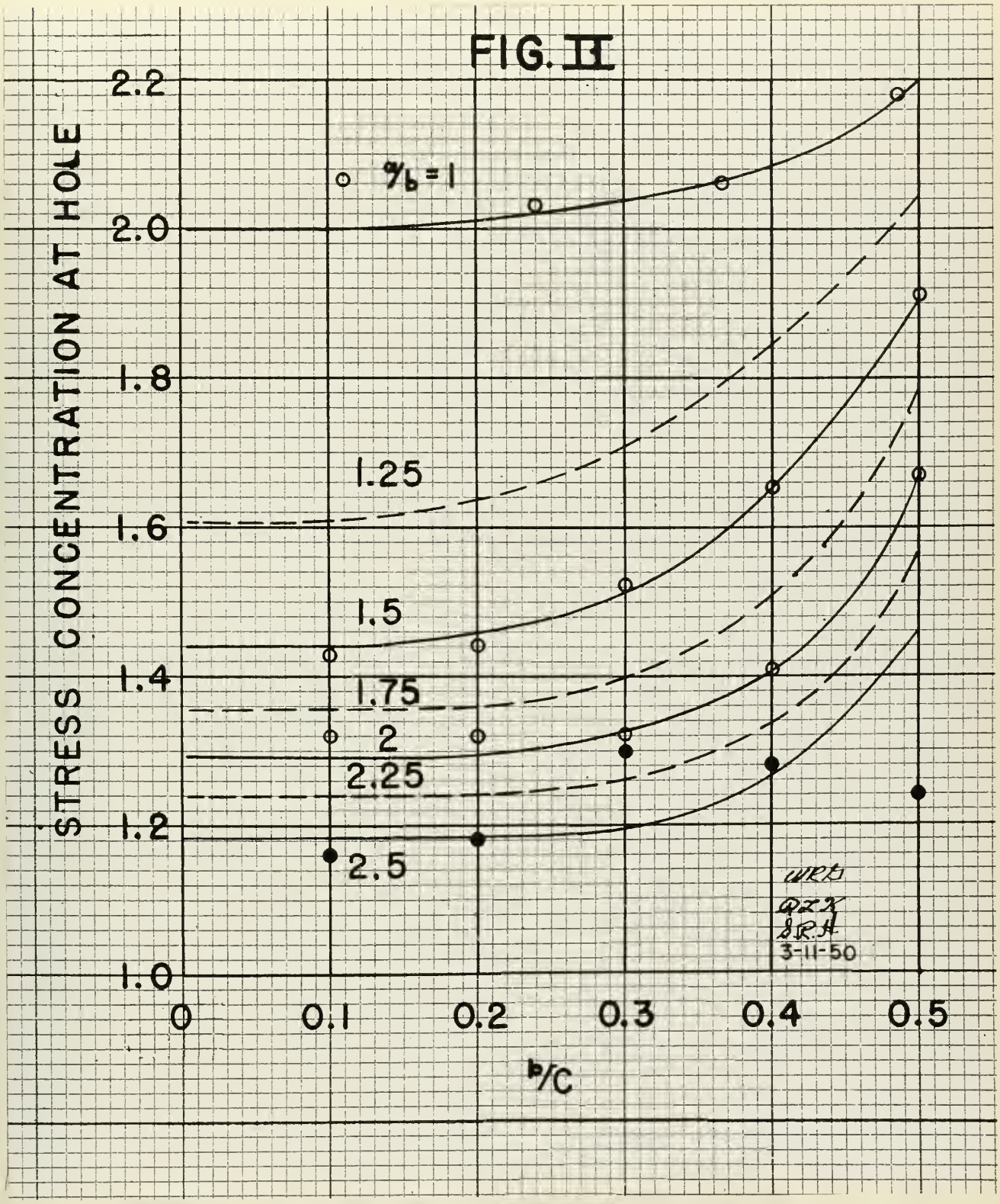
FIG. II
STRESS CONCENTRATION AT HOLE
2.2
2.0
1.8
1.6
1.4
1.2
1.0
0
0.1
0.2
0.3
0.4
0.5
b/c
a/b = 1
1.25
1.5
1.75
2
2.25
2.5
WRD
QZZ
SRH
3-11-50

FIG. III

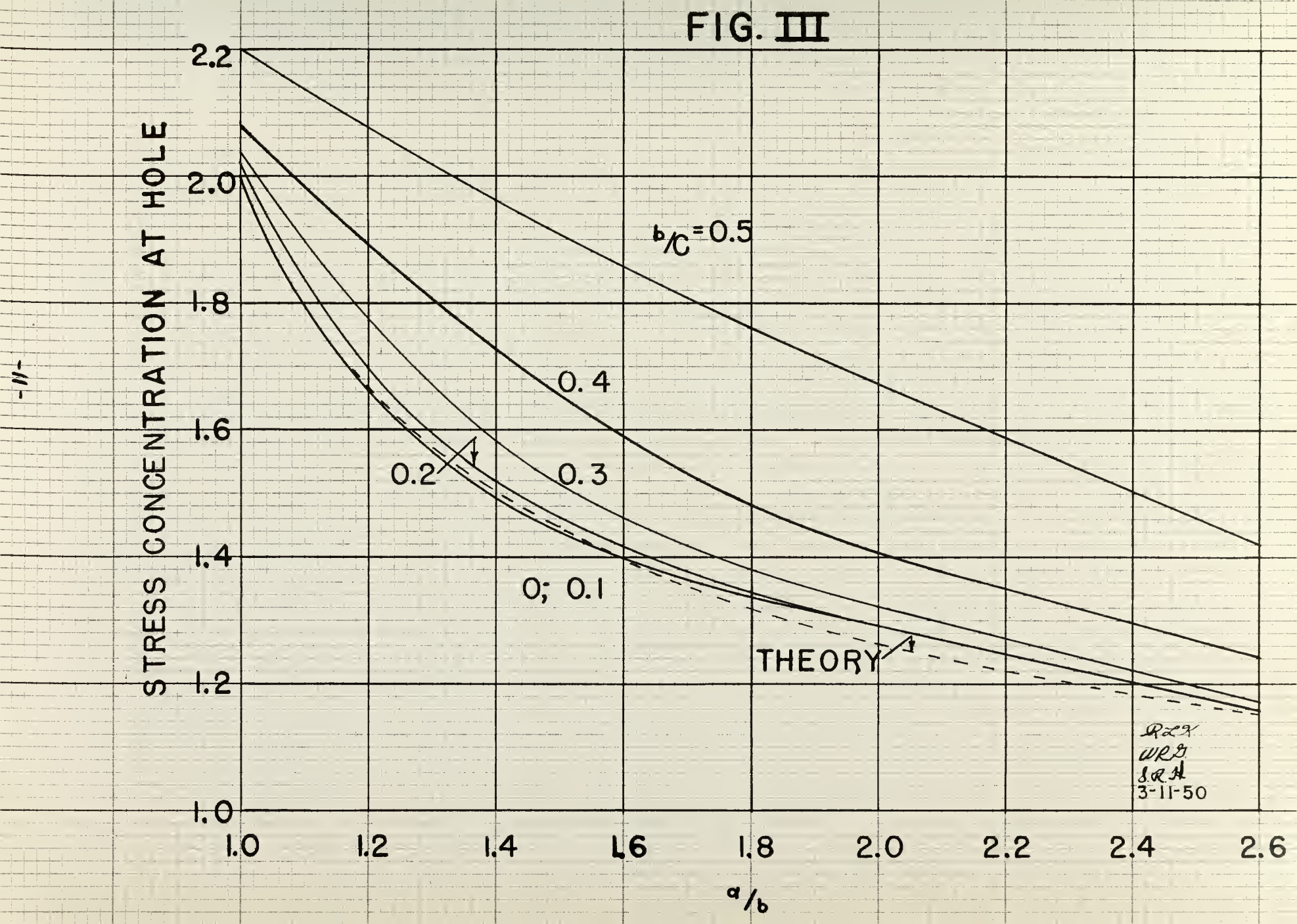
STRESS CONCENTRATION AT HOLE
2.2
2.0
1.8
1.6
1.4
1.2
1.0
1.0
1.2
1.4
1.6
1.8
2.0
2.2
2.4
2.6
a/b
b/c = 0.5
0.4
0.3
0.2
0; 0.1
THEORY
RLX
WRG
SRH
3-11-50

FIG. V

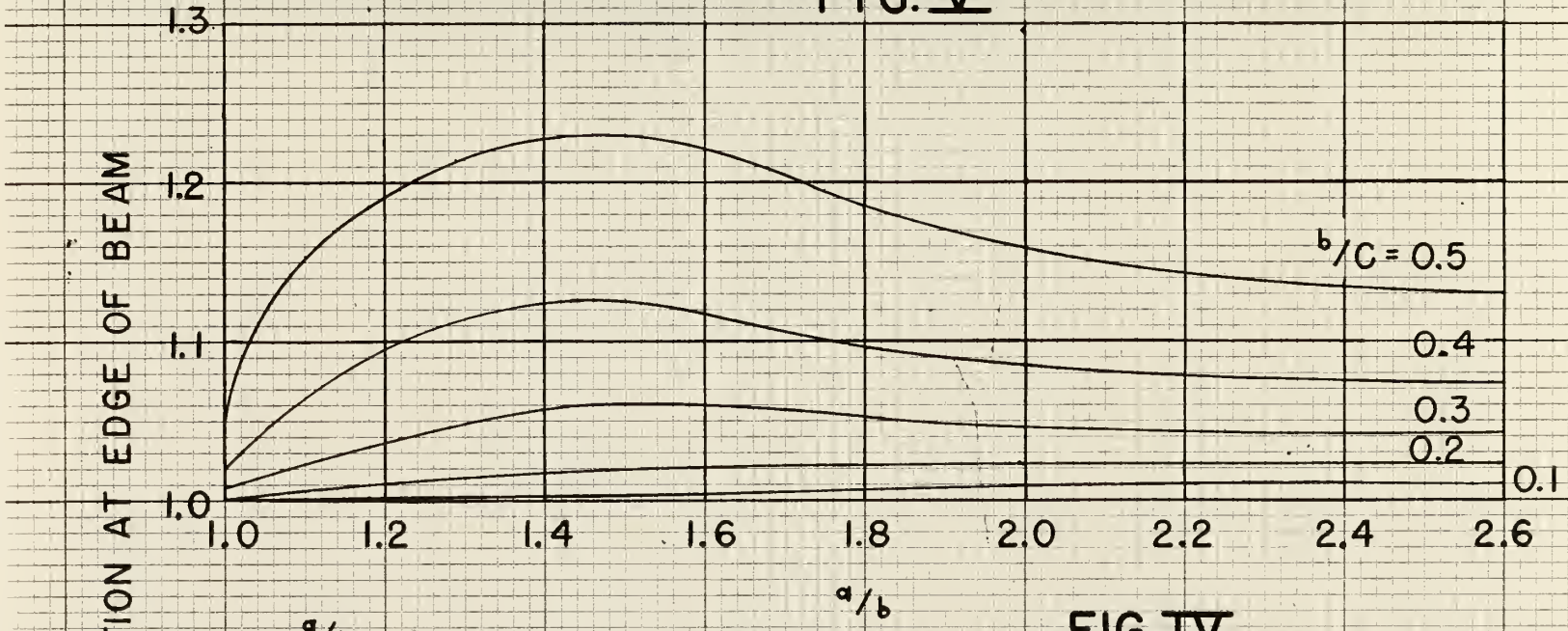
STRESS CONCENTRATION AT EDGE OF BEAM
1.3
1.2
1.1
1.0
1.0
1.2
1.4
1.6
1.8
2.0
2.2
2.4
2.6
a/b
b/C = 0.5
0.4
0.3
0.2
0.1

FIG. IV

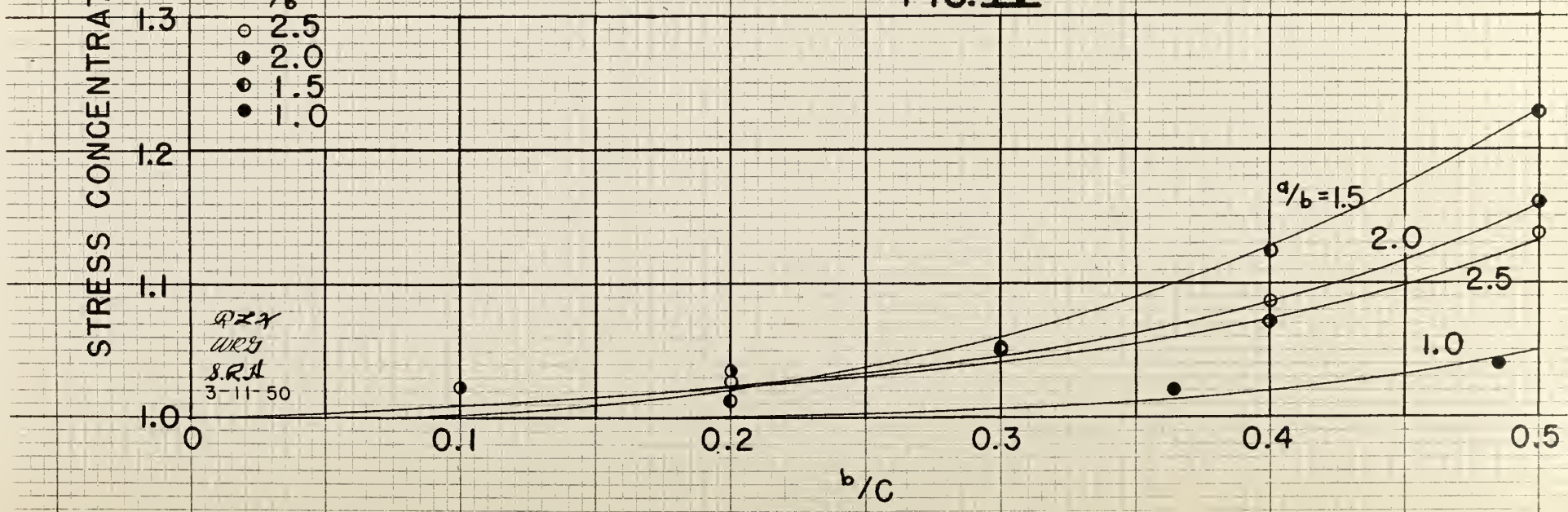
STRESS CONCENTRATION AT EDGE OF BEAM
a/b
2.5
2.0
1.5
1.0
1.3
1.2
1.1
1.0
RZY
WRY
S.R.A
3-11-50
0
0.1
0.2
0.3
0.4
0.5
b/C
a/b = 1.5
2.0
2.5
1.0

DISCUSSION OF RESULTS

The curves shown in Figures II and III, and IV and V respectively represent the cross-fairing of the data incorporated in Table I. The results of Figures II and III are consistent with the well-verified facts that a small crack in the longitudinal direction of a beam causes a stress concentration of unity and a small crack in the transverse direction of the beam causes an infinite stress concentration. This character is shown again in the slope of the curves of Figures III. It is not surprising, either, that the circular opening causes a greater stress concentration than any of the other flat ovaloids (no ovaloids transverse to the axis of the beam were tested). This result is similar in content to a comparison of (1) with (2) and of (6) with (4).

The curves of Figures IV and V are not so easily explained. At the outset there appears to be no rational reason for the apparent maximum stress concentration factor at the edge of the beam for a ratio of length to depth of opening of 1.5. The almost perfect agreement of the experimental results with the theoretical solution for the value of the ratio of depth of opening to depth of beam of zero and for all values of such ratio for the circular opening lend confidence in the remaining experimental work. On this basis the authors feel safe in predicting that the maximum augmentation of stress caused by a small opening of this type will occur when the ratio of length to depth of opening is in the vicinity of 1.5. This same confidence enables the authors to conclude that the ratio of depth of opening to depth of beam should lie between 1/4 and 1/3 if no material increase in the stress concentration at the edge of the hole is desired.

CONCLUSIONS

1. The stress concentration factor at the edge of the hole varies inversely with the ratio of length to depth of opening and directly with the ratio of depth of opening to depth of beam.

2. The stress concentration factor at the edge of the beam varies directly with the ratio of depth of opening to depth of beam, but in some complex manner with the ratio of length to depth of hole.

3. The critical value of the ratio of length to depth of opening falls in the vicinity of 1.5. The critical value of the ratio of depth of opening to depth of beam lies in the neighborhood of 1/4 to 1/3. The critical value is that value at which a small increase in the aforementioned ratio is accompanied by a relatively large increase in the stress concentration factor at the edge of the hole.

4. The theoretical solution developed in (8) and in the APPENDIX is satisfactory for purposes of engineering design.

5. The photoelastic method is well-suited for inexpensive and rapid determination of stress concentration factors.

RECOMMENDATIONS

1. Further experimental investigations for values of the ratio of length to depth of opening in the vicinity of 1.5 seem highly desirable to fix this critical value.

2. Further experimental and theoretical investigations in this nature to determine the effect of reinforcement of such openings and the nature of complex bending; that is, bending with shear, seem desirable.

3. In the absence of a clearly defined "no load" picture in a photoelastic investigation, it is recommended that small but appreciable stress be introduced to clarify the basic pattern.

APPENDIX

APPENDIX A

DETAILS OF PROCEDURE

Description of Models

Four (4) basic models were prepared. Each was fitted with an interior hole 1/4 inches in the transverse direction, but the longitudinal extent were respectively, 1/4 inches, 3/8 inches, 1/2 inches, and 5/8 inches. The distance between suspension points was maintained at 11 1/8 inches; the distance from suspension points to the loading points was maintained at 5 inches. Each of these models was successively diminished in depth in order to obtain the increasing values of the ratio of depth of opening to depth of beam. Only in the case of the circular opening was it necessary to recut the interior hole. The particulars of the various models and the loads to which they were subjected are summarized in Table II.

TABLE II

Summary of Model Particulars

Hole Dimensions	Depth of Beam	b/c	Load in lbs.	a/b
1/4" x 1/4"	2.240	0.1115	85.35	1.0
1/2 x 1/2	2.094	0.239	85.35	1.0
1/2 x 1/2	1.372	0.364	46.00	1.0
1/2 x 1/2	1.030	0.485	22.00	1.0
1/2 x 1/2	0.833	0.600	4.00	1.0
1/4 x 3/8	2.500	0.100	85.35	1.5
1/4 x 3/8	1.2500	0.200	20.00	1.5
1/4 x 3/8	0.833	0.300	9.00	1.5
1/4 x 3/8	0.625	0.400	4.0	1.5
1/4 x 3/8	0.500	0.500	1.50	1.5
1/4 x 1/2	2.500	0.100	85.35	2.0
1/4 x 1/2	1.250	0.200	20.00	2.0
1/4 x 1/2	0.833	0.300	9.00	2.0
1/4 x 1/2	0.625	0.400	4.00	2.0
1/4 x 1/2	0.500	0.500	1.50	2.0
1/4 x 5/8	2.500	0.100	56.90	2.5
1/4 x 5/8	1.250	0.200	18.50	2.5
1/4 x 5/8	0.833	0.300	9.50	2.5
1/4 x 5/8	0.625	0.400	6.00	2.5
1/4 x 5/8	0.500	0.500	5.00	2.5

Methods of Analysis

Standard photoelastic methods were used, supplemented where required with direct analytic methods. A transverse section was chosen a minimum of two lengths removed from the longitudinal end of the hole. The condition of stress at this section should, according to St. Venant* be removed from the influence of the hole. This section was designated, accordingly, "pure bending", see Figs. VI, VII, VIII, and IX, and was the reference condition for determining the stress concentration factors.

Examination of the photographs, Figs. X, XI, XII, and XIII, revealed that the maximum stress at the edge of the hole occured at its vertical axis of symmetry, designated "diameter"; whereas the maximum stress at the edge of the beam occured vertically above the longitudinal end of the opening, designated "end of hole." It was therefore necessary to determine the fringe order existing at the free boundaries in these two locations. Since a fringe is the locus of points of constant difference between principal stresses, one of which must be zero at a free boundary, no other experimental information was necessary for the evaluation of actual stress existing at these free boundaries. Fortunately, the "exact," mathematical, stress analysis for pure bending also reveals that one principal stress is also zero everywhere, which fact obviated any additional information for the pure bending condition as well. Thus the desired stress concentration factor was merely the ratio of the fringe order actually measured at a given point to the fringe order determined at the corresponding depth in the pure bending condition. Both fringe orders referred

---

* Ref. (9), p. 31

to above must be the actual value determined by the photograph corrected for any residual stress in the "no load" condition.

This correction is shown in Figures VI, VII, VIII, and IX as the difference between the dotted and solid lines. The case of pure bending was obtained by plotting integral fringe orders, solid lines in the photographs, at the proper fraction of depth from the bottom. The upper and lower halves of the beam were handled separately, since, in pure bending, one half would be in tension and the other in compression, with zero stress at the middle surface. The best straight line, guided here by the theoretical linear distribution of bending stresses, was passed through the experimental points in each half of the beam. It will be observed in Figures VI, VII, VIII, and IX that in no case did these lines pass through zero at the middle surface. Shifts of both halves of these lines effected to make the lines pass through this zero point and to intercept the same value at the edges of the beam. It will be noted from the figures that in most cases this was almost a parallel shift of lines with approximately the same values for both halves of the beam. This amount of shift, in all but the shallowest models, was of the same character as the load stress and less than fringe order 1. This represents the residual stress in the specimen, which from the density of blackness in the "no load" picture, must be very nearly constant over the section. It may be noted, however, that in the shallowest beams there is appreciable residual stress, more than a single fringe order and of the same character to the load stress. This condition is caused by the bending effect of the end brackets and admits a more straightforward correction procedure.

The "diameter" and "end of hole" curves have this same correction factor applied to them in all cases except for the circular opening, Figure VI and X. This procedure was followed since the density of blackness on the "no load" picture appeared to be the same throughout these specimens except for insignificant surface blemishes. The circular openings retained machining stresses for a considerable period of time. The fringes representing these machining stresses were concentric rings which permitted a plot of fringe order versus fraction of depth from the bottom, see Figure VI. These values were then added algebraically to the experimentally determined values, previously plotted. The character of the machining stress was easily determined by noting the "bulging" or "depressing" effect on the fringes in the loaded condition. For example when fringes observed in the compression half of the beam were "depressed" toward the hole and bent away from the diameter toward the end of the hole, thus increasing the fringe order at the diameter of the hole, the machining stress was obviously compression and should be subtracted from the experimentally determined value to obtain the actual fringe order caused by the bending alone. Conversely, if, in the compression half of the beam, fringes were "bulged" away from the edge of the hole, causing dips on either side of the diameter, the machining stress was tension and should be added to the experimentally determined value to obtain the actual fringe order caused by the bending alone.

A polar plot to obtain the experimental fringe order at the diameter of the circular hole was used in an effort to ascertain this peak value with greater accuracy. This is shown in Figure VI. The

photograph was tacked to a drawing board and the center of the hole determined. Radial lines were then passed from the center of the circle through the intercepts of the fringes at the circumference. The angles were then transferred to the plot and the correct value of fringe order was plotted radially on this line. Finally, a smooth curve was passed through the points and the value of the fringe order determined on the diameter extended. This gave the desired end point of the curve.

APPENDIX B

APPENDIX B

Sample Calculations

The data are summarized in entirety in Table I of RESULTS. Figures VI, VII, VIII, and IX, referred to in APPENDIX A., are shown to illustrate the methods of analysis and typical calculations of stress concentration factors. One sample from each series of models is included; that is, one for each ratio of length to depth of opening and each ratio of depth of opening to depth of beam.

FIG. VI

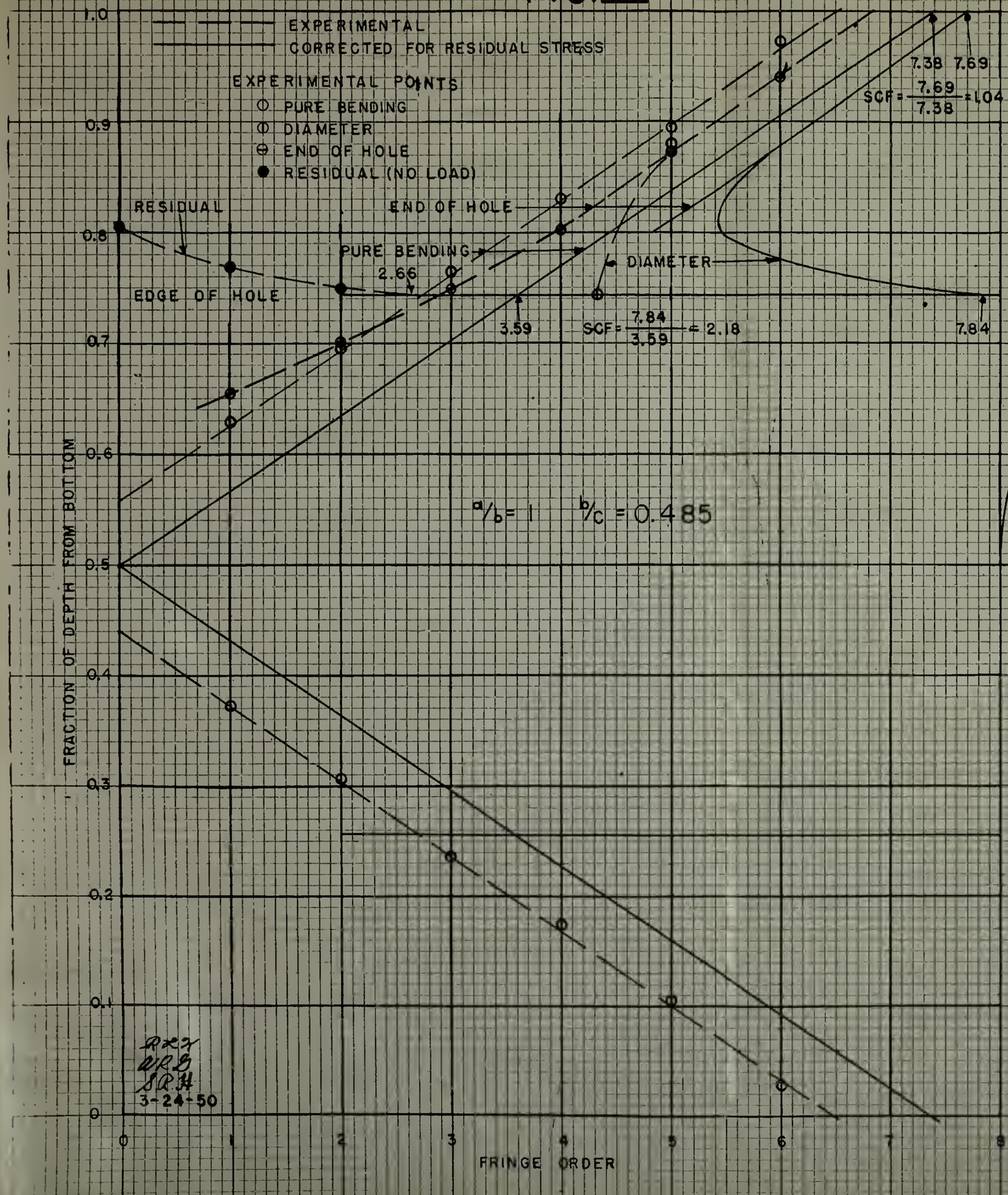

RKZ
DRS
SRH
3-24-50

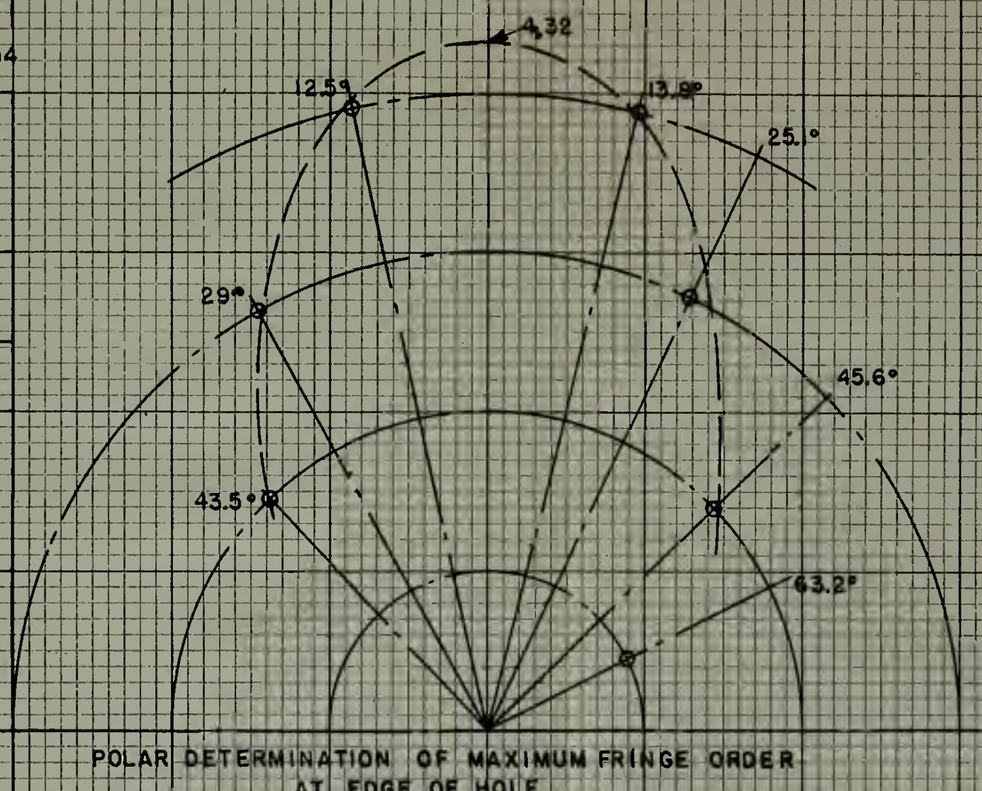

POLAR DETERMINATION OF MAXIMUM FRINGE ORDER AT EDGE OF HOLE

FIG. VII

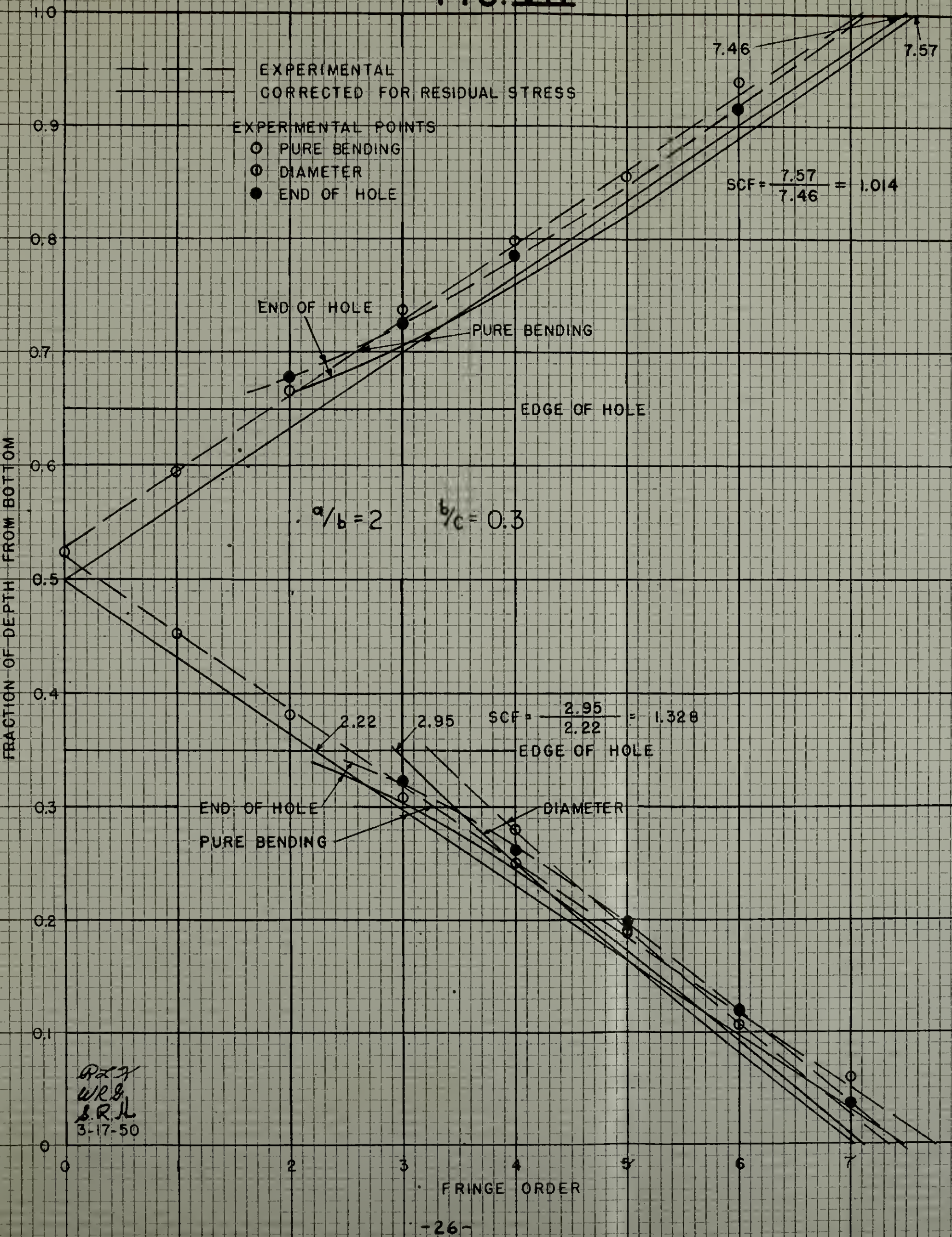

RZT
WRG
S.R.L
3-17-50

CROSS SECTION 10 X 10

FIG. VIII

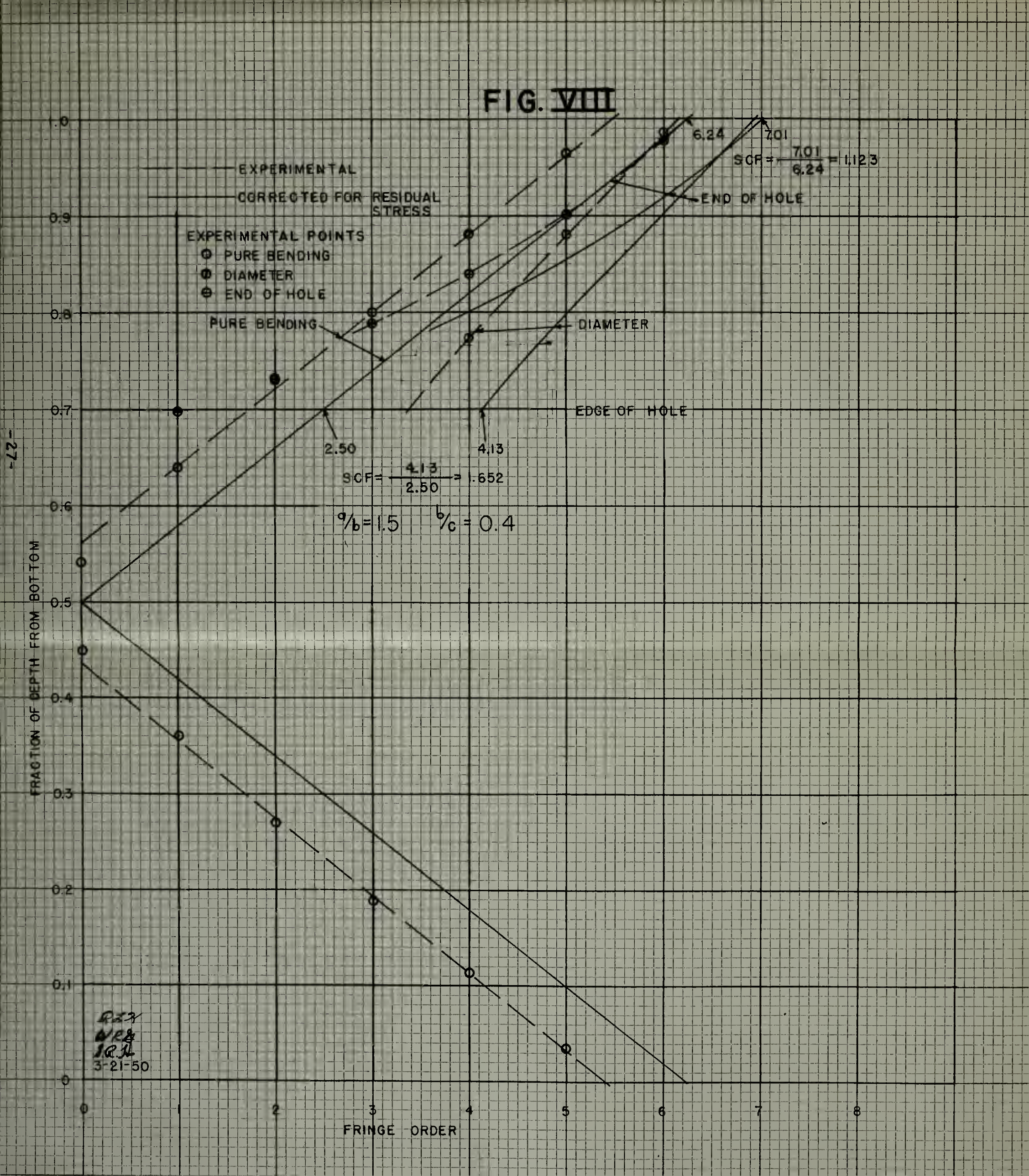

R.S.I.
A.E.A.
J.C.L.
3-21-50

FIG. IX

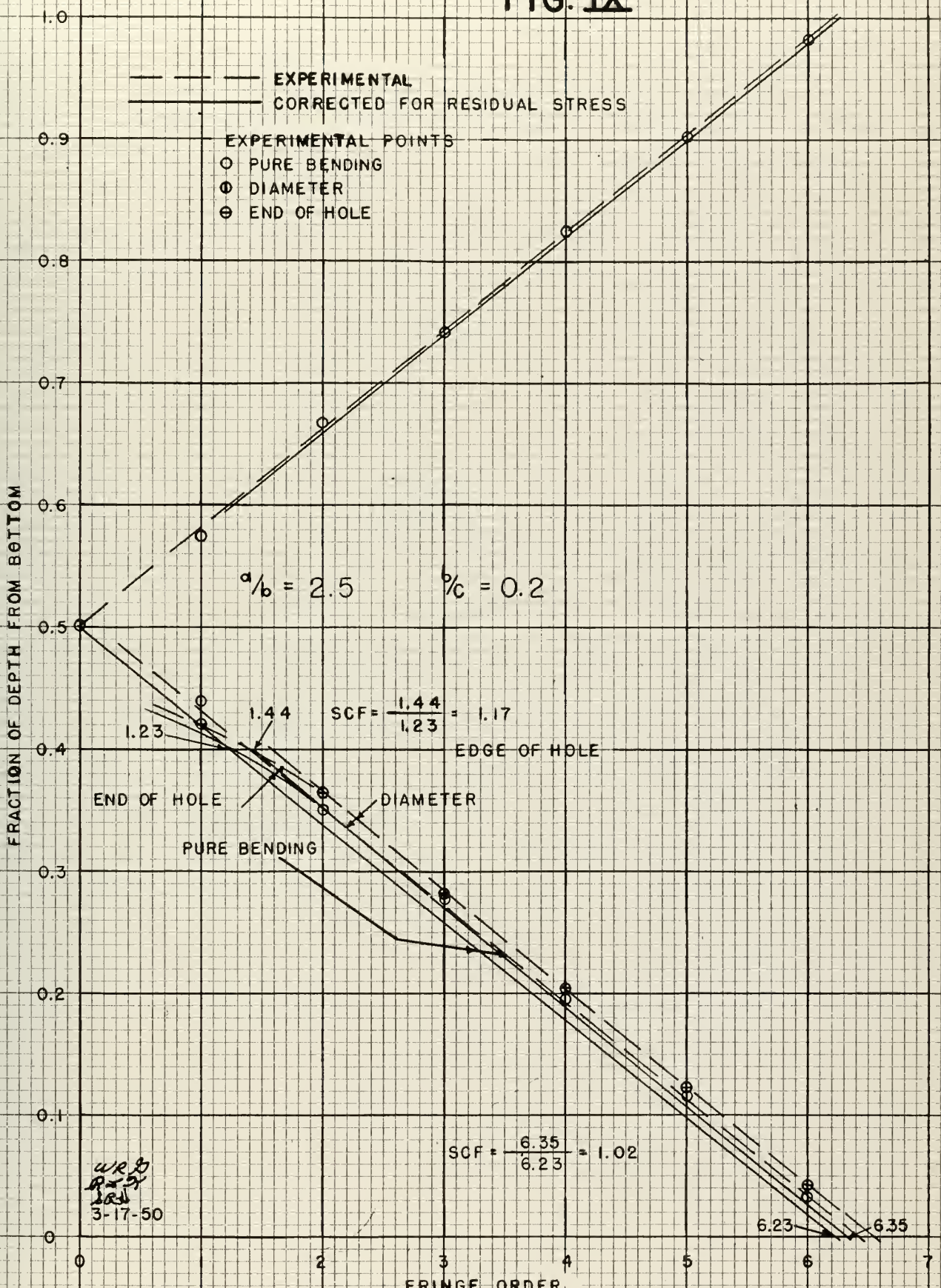
EXPERIMENTAL
CORRECTED FOR RESIDUAL STRESS
EXPERIMENTAL POINTS
PURE BENDING
DIAMETER
END OF HOLE
a/b = 2.5
b/c = 0.2
1.23
1.44
SCF = 1.44/1.23 = 1.17
EDGE OF HOLE
END OF HOLE
DIAMETER
PURE BENDING
SCF = 6.35/6.23 = 1.02
6.23
6.35
WRB
A-57
JRJ
3-17-50
FRACTION OF DEPTH FROM BOTTOM
FRINGE ORDER
0
0.1
0.2
0.3
0.4
0.5
0.6
0.7
0.8
0.9
1.0
2
3
4
5
6
7

APPENDIX C

APPENDIX C

Original Data

The original data is presented in the form of photographs of the "no load" and load conditions. Each page of photographs includes all the pictures taken for a given series of models: Figure X for the ratio of length to depth of opening of 1, Figure XI for the ratio of 1.5, Figure XII for 2, and Figure XIII for 2.5.

b/C = 0.600 No Load

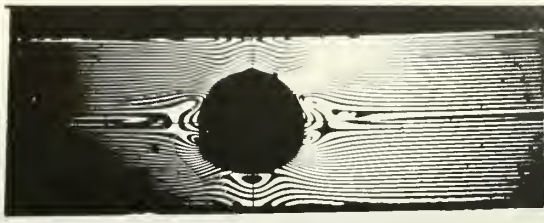

b/C = 0.600 Load

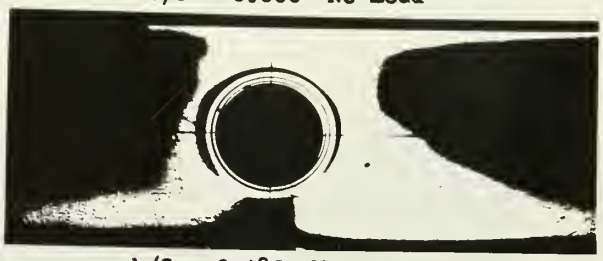

b/C = 0.485 No Load

b/C = 0.485 Load

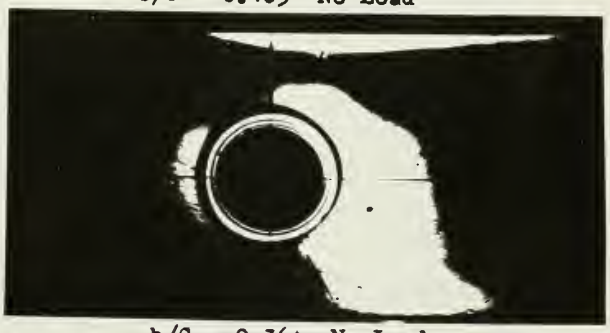

b/C = 0.364 No Load

b/C = 0.364 Load

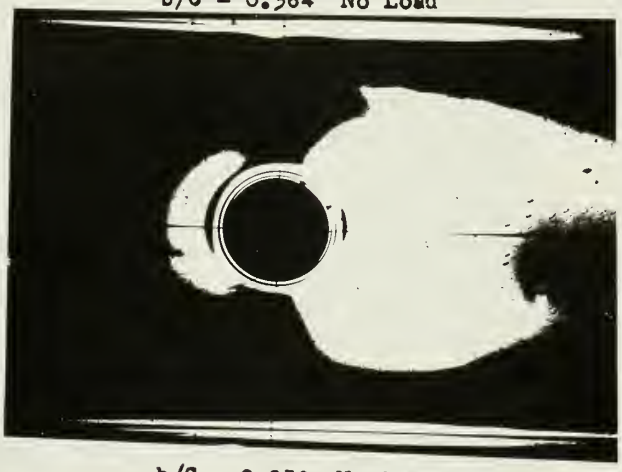

b/C = 0.239 No Load

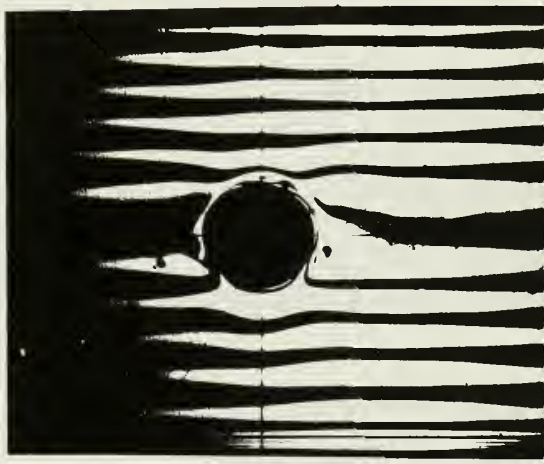

b/C = 0.239 Load

a/b = 1

FIG. X

b/C = 0.1115 Lo

FIG. XI

b/C = 0.5 No Load

b/C = 0.5 Load

b/C = 0.4 No Load

b/C = 0.4 Load

b/C = 0.3 No Load

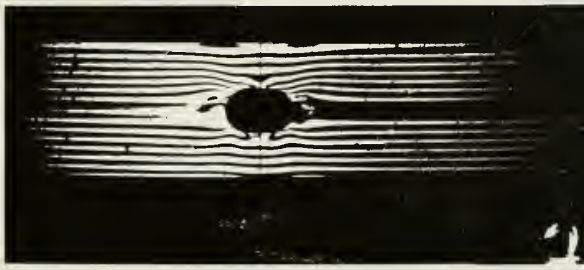

b/C = 0.3 Load

b/C = 0.2 No Load

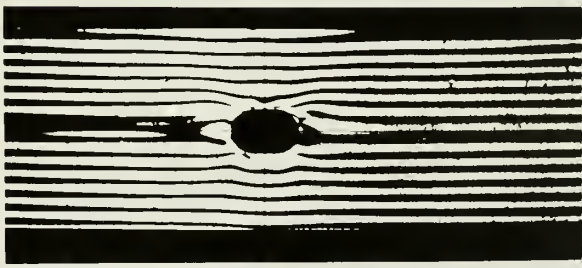

b/C = 0.2 Load

b/C = 0.1 No Load

a/b = 1.5

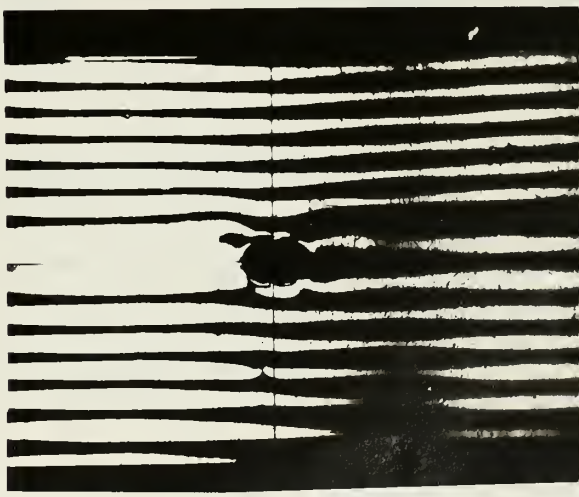

b/C = 0.1 Load

FIG. XII

b/C = 0.5 No Load

b/C = 0.5 Load

b/C = 0.4 No Load

b/C = 0.4 Load

b/C = 0.3 No Load

b/C = 0.3 Load

b/C = 0.2 No Load

b/C = 0.2 Load

b/C = 0.1 No Load

b/C = 0.1 Load

a/b = 2

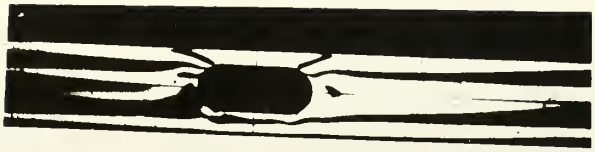

b/C = 0.5 No Load

b/C = 0.4 No Load

a/b = 2.5

FIG. XIII

b/C = 0.5 Load

b/C = 0.4 Load

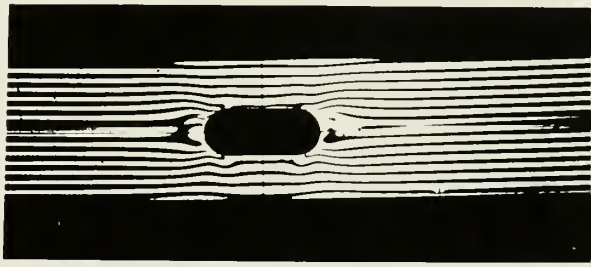

b/C = 0.3 Load

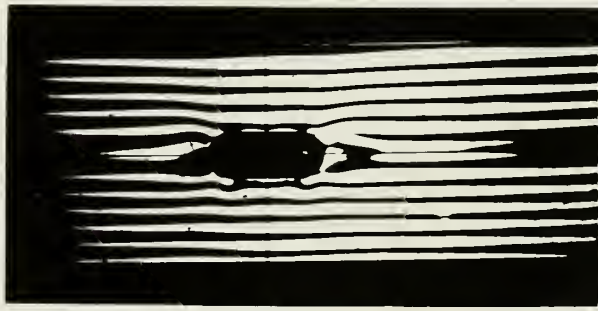

b/C = 0.2 Load

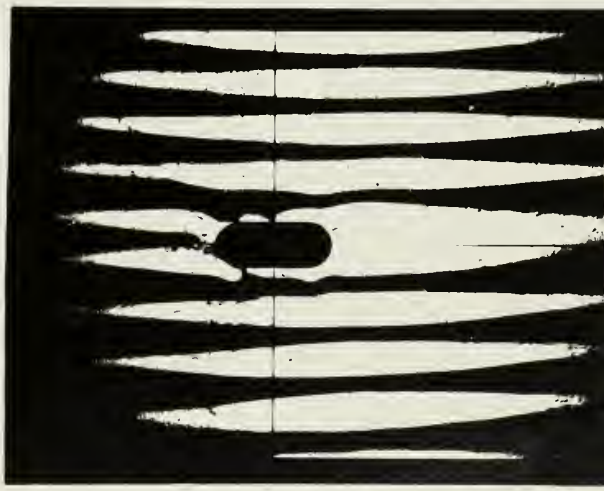

b/C = 0.1 Load

APPENDIX D

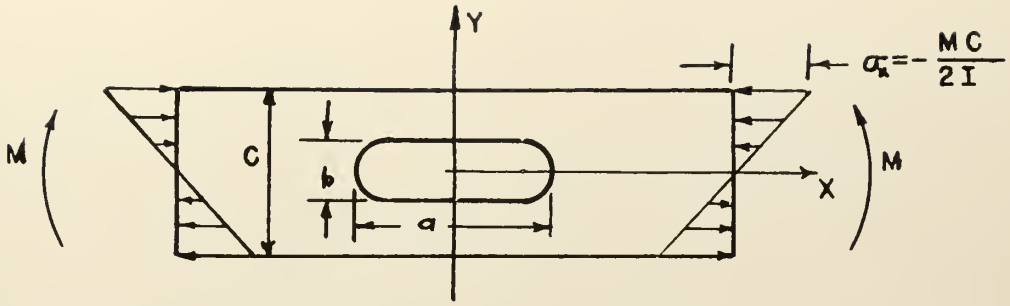

FIG. XIV

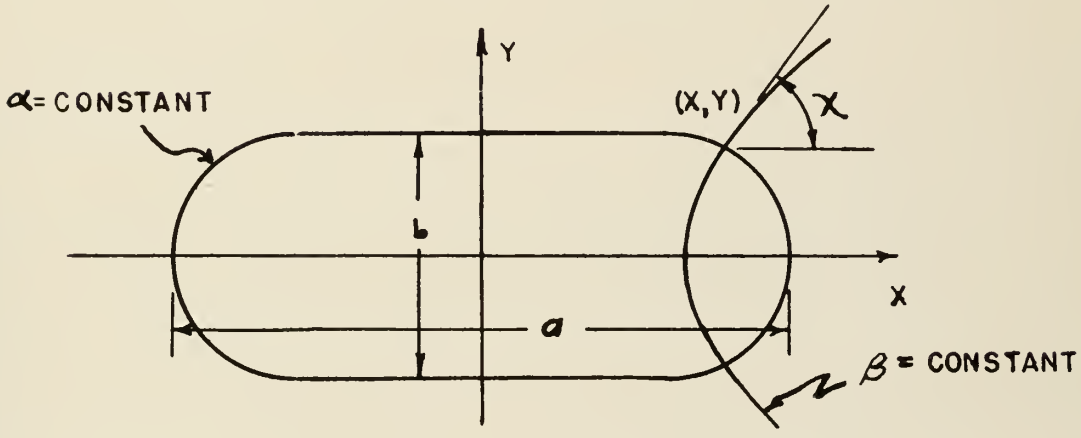

FIG. XV (a) Z-PLANE

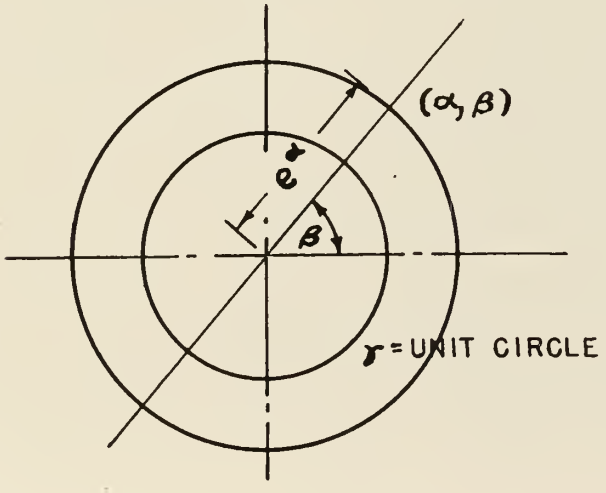

FIG. XV (b) ζ PLANE

RLX
WRB
S.R.H.
4-6-50

APPENDIX D

Nomenclature

(x,y) = Cartesian co-ordinates

(α,β) = Orthogonal curvilinear coordinates

$z = x + iy$

$w = \alpha + i\beta$

$\zeta = e^{w}$

h = stretch ratio

$\lambda = e^{i\beta}$

γ = angle in z-plane between tangent to curve β = constant and x-axis

s, t, R = real parameters

$T = t + \frac{Rt}{s} - s$

Φ, Ψ = potential functions of complex variable z

φ, ψ = potential function of complex variable

F = Airy stress function

$\sigma_x, \sigma_y, \sigma_\alpha, \sigma_\beta$ = normal stresses; σ_x is normal to surface for which x = constant, etc.

$\tau_{xy}, \tau_{\alpha\beta}$ = shear stresses

A_n, B_n, a_n, b_n = complex constants

M = applied bending moment

y_o = half-height of opening at x = 0

$= s - t + R$

I = moment of inertia of beam

$\_$ = bar above, indicates conjugate complex

SCF = stress concentration factor

Development of Theoretical Solution[3]

Consider a function: $z = f(\zeta)$ (1)

which transforms continuously points in the $\zeta(\alpha, \beta)$ plane into points in the $z(x,y)$ plane. Here $z = x + iy$ and $\zeta = e^{\alpha+i\beta} = e^{w}$.

In particular, see Figs. XV(a) and (b), points on the circle of radius e^{α}, with α held constant, defined by a position angle β, will transform into points (x,y) on a closed curve defined by the functional form (1). The radial line defined by β = constant transforms into a curve orthogonal to those for which α = constant. The case of $\alpha = 0$ is important; it defines the unit circle, γ, in the ζ-plane and transforms, by the proper selection of the form of (1), into the shape of the opening to be studied. A special symbol λ will be assigned to those ζ-values which lie on this circle:

$$\lambda = e^{i\beta} \qquad (2)$$

so that the conjugate of λ : $\bar{\lambda} = e^{-i\beta} = 1/\lambda$.

The transformation defined by Equation (1) describes the relation between an increment dz in the z-plane and an increment dw in the ζ-plane. The ratio, expressed in polar form:

$$\frac{dz}{dw} = he^{i\psi} \qquad (3)$$

3 - This development follows that of (8) and was largely guided by Mr. J. S. Brock.

defines h the stretch ratio, and χ , the angle between the tangent to the curve β = constant and the x-axis; see [10] , Article 2.32. h and χ are obtained by differentiating (1):

$$\frac{dz}{dw} = \frac{dz}{d\zeta} \cdot \frac{d\zeta}{dw} = \frac{dz}{d\zeta} \zeta \qquad (4)$$

Equating (3) and (4):

$$h\, e^{i\chi} = \zeta \frac{dz}{d\zeta} = \zeta\, z'(\zeta) \qquad (5)$$

where the prime indicates differentiation with respect to the variable in the parenthesis.

Thus, the conjugate of (5) is:

$$h\, e^{-i\chi} = \bar{\zeta}\, z'\left(\frac{1}{\zeta}\right) \qquad (6)$$

provided (1) has real coefficients and parameters.

Multiplication of (5) and (6) gives:

$$h^2 = z'(\zeta) z'(\bar{\zeta})\, \zeta\, \bar{\zeta} = z'(\zeta) z'(\bar{\zeta}) e^{2a} \qquad (7)$$

The division of (5) by (6) gives:

$$e^{2i\chi} = \frac{z'(\zeta)}{z'(\bar{\zeta})} e^{2i\beta}. \qquad (8)$$

In general, in plane problems of elasticity, the technique which follows can be applied to any real rational mapping function $z = f(\zeta)$; that is, where z is the ratio of two polynomials in ζ havin real coefficients.

Consider the mapping function due to Greenspan [7] :

$$z = s\zeta + \frac{t}{\zeta} + \frac{R}{\zeta^3} \qquad (9)$$

where s, t, and R are real constants that are determined from the proportions of the opening, and $z = x + iy$ and $\zeta = e^{\alpha+i\beta}$.

Then: $x + iy = se^{\alpha} \cdot e^{i\beta} + te^{-\alpha} \cdot e^{-i\beta} + Re^{-3\alpha} \cdot e^{-3i\beta}$

$$= (se^{\alpha} + te^{-\alpha})\cos\beta + Re^{-3\alpha}\cos 3\beta + i(se^{\alpha} - te^{-\alpha})\sin\beta - iRe^{-3\alpha}\sin 3\beta.$$

Equating the real and imaginary parts separately:

$$x = (se^{\alpha} + te^{-\alpha})\cos\beta + Re^{-3\alpha}\cos 3\beta$$
$$y = (se^{\alpha} - te^{-\alpha})\sin\beta - Re^{-3\alpha}\sin 3\beta \qquad (10)$$

When $\alpha = 0$, Equations (10) define the general ovaloid opening:

$$x = (s + t)\cos\beta + R\cos 3\beta$$
$$y = (s - t)\sin\beta - R\sin 3\beta \qquad (10a)$$

Several special cases are of interest:

(a) When R = 0, an ellipse is defined.

(b) When R = t = 0, a circle of radius s is defined.

(c) When t = 0 and R < 0, a square with fillets at the corners is approximated.

(d) When t = 0 and R > 0, the square is rotated 45°.

In the general case, by the proper choice of s, t, and R, the

equations can be made to approximate the common structural openings, specifically the one composed of a rectangle with semicircles at each end.

From (9): $$z'(\zeta) = s - \frac{t}{\zeta^2} - \frac{3R}{\zeta^4} \qquad (11)$$

Now h and γ can be determined from (7) and (8). When $\alpha = 0$, corresponding to the opening, the subscript zero is used and from (7):

$$h_o^2 = z'(\lambda)z'(\bar{\lambda}) = (s - \frac{t}{\lambda^2} - \frac{3R}{\lambda^4})(s - \frac{t}{\bar{\lambda}^2} - \frac{3R}{\bar{\lambda}^4})$$
$$= s^2 + t^2 + 9R^2 - (2st - 6Rt)\cos 2\beta - 6Rs\cos 4\beta \qquad (12)$$

In order to obtain stresses in plane problems of elasticity by using the complex variable method, two potential functions must be determined. These functions can be expressed as:

$$\Phi(z) = \sum_{1}^{\infty} A_n z^n + \sum_{1}^{\infty} a_n/z^n$$
$$\Psi(z) = \sum_{1}^{\infty} B_n z^n + \sum_{1}^{\infty} b_n/z^n \qquad (13)$$

where, A_n, a_n, B_n, and b_n are constants, possibly complex. The solution is thus reduced to the evaluation of these constants. The stress condition at one boundary, infinity, will determine A_n and B_n; the stress condition at the other boundary, the opening, will determine a_n and b_n. Once the two potential functions are completely determined, the stresses in the plane may be determined by differentiation. Thus, these functions are counterparts of the Airy stress function. In fact, the

Airy stress function corresponding to these potential functions is given by:

$$F(x,y) = \text{Real Part of}\left[\bar{z}\ \Phi(z) + \int \Psi(z)dz\right] \qquad (14)$$

The stresses can be found in terms of the two functions:

$$\sigma_x + \sigma_y = 2\left[\Phi'(z) + \bar{\Phi}'(\bar{z})\right]$$

$$\sigma_y - \sigma_x + 2i\tau_{xy} = 2\left[\bar{z}\ \Phi''(z) + \Psi'(z)\right] \qquad (15)$$

The usual transformation equations[4] give:

$$\sigma_\alpha + \sigma_\beta = \sigma_x + \sigma_y$$

$$(\sigma_\beta - \sigma_\alpha + 2i\tau_{\alpha\beta})e^{-2i\chi} = \sigma_y - \sigma_x + 2i\tau_{xy} \qquad (16)$$

By combining Equations (8), (15), and (16):

$$\sigma_\alpha + \sigma_\beta = 2\left[\Phi'(z) + \bar{\Phi}'(\bar{z})\right] \qquad (17)$$

$$\sigma_\beta - \sigma_\alpha + 2i\tau_{\alpha\beta} = 2\left[z(\zeta)\,\Phi''(z) + \Psi'(z)\right]\frac{z'(\zeta)}{z'(\bar{\zeta})}\,e^{2i\beta}$$

where the functions of z are to be expressed in terms of $\zeta(\alpha, \beta)$:

$$\begin{aligned}\Phi(z) &= \Phi\left[z(\zeta)\right] = \varphi(\zeta)\\ \Psi(z) &= \Psi\left[z(\zeta)\right] = \varphi(\zeta)\end{aligned} \qquad (18)$$

Differentiation is with respect to the variable in parentheses:

4 - Ref. [10], p. 135

$$\Phi'(z) = \frac{\varphi'(\zeta)}{z'(\zeta)}$$

$$\Psi'(z) = \frac{\psi'(\zeta)}{z'(\zeta)} \qquad (19)$$

$$\Phi''(z) = \frac{\varphi''(\zeta)}{[z'(\zeta)]^2} - \frac{\varphi'(\zeta) z''(\zeta)}{[z'(\zeta)]^3}$$

If, at the opening, the normal stress σ_α and the shear stress $\tau_{\alpha\beta}$ are zero, which is the case at a free boundary, it can be shown that:

$$\varphi(\lambda) + \frac{z(\lambda)}{z'(\frac{1}{\lambda})} \bar{\varphi}'(\frac{1}{\lambda}) + \bar{\psi}(\frac{1}{\lambda}) = 0 \qquad (20)$$

The functions $\varphi(\zeta)$ and $\psi(\zeta)$ may be evaluated with the use of the Cauchy Theorems regarding poles and residues.[5]

From [12], these are:

Theorem I. If $f(\zeta)$ is continuous in the closed region $|\zeta| \leq 1$ and analytic in the interior with the possible exception of the point $\zeta = 0$, where $f(\zeta)$ has the form

$$f(\zeta) = \frac{A_1}{\zeta} + \frac{A_2}{\zeta^2} + \cdots + \frac{A_n}{\zeta^n} + g(\zeta)$$

and $g(\zeta)$ is analytic; then:

$$\frac{1}{2\pi i} \int_\gamma \frac{f(\lambda)}{\lambda - \zeta} d\lambda = -\frac{A_1}{\zeta} - \frac{A_2}{\zeta} - \cdots - \frac{A_n}{\zeta^n}$$

for $|\zeta| > 1$

where γ is the unit circle $\gamma = e^{i\beta}$.

5 - Ref. [11], pp. 144-145

Theorem II. If $f(\zeta)$ is continuous in the closed region $|\zeta| \geq 1$ and analytic in the region exterior to λ, with the possible exception of the point $\zeta = \infty$, where $f(\zeta)$ has the form

$$f(\zeta) = A_o + A_1\zeta + A_2\zeta + \ldots + A_n\zeta^n + \sum_{K}^{\infty} \frac{B_K}{\zeta^K}$$

Then:

$$\frac{1}{2\pi i}\int_r \frac{f(\lambda)}{\lambda-\zeta}d\lambda = -f(\zeta) + A_o + A_1\zeta + A_2\zeta^2 + \ldots + A_n\zeta^n \qquad \text{for } |\zeta| > 1$$

Consider Equations (13):

$$\Phi'(z) = \sum_{1}^{k} nA_n z^{n-1} + \sum_{1}^{\infty} -\frac{na_n}{z^{n+1}}$$

$$\Phi''(z) = \sum_{1}^{k} n(n-1)A_n z^{n-2} + \sum_{1}^{\infty} \frac{n(n+1)a_n}{z^{n+2}}$$

$$\Psi'(z) = \sum_{1}^{k} nB_n z^{n-1} + \sum_{1}^{\infty} -\frac{nb_n}{z^{n+1}}$$

Now let z approach infinity in the x-direction:

$$\Phi'(z)_{x=\infty} = \left[\sum_{1}^{k} nA_n z^{n-1}\right]_{x=\infty}$$

$$\Phi''(z)_{x=\infty} = \left[\sum_{1}^{k} n(n-1)A_n z^{n-2}\right]_{x=\infty} \qquad (21)$$

$$\Psi'(z)_{x=\infty} = \left[\sum_{1}^{k} nB_n z^{n-1}\right]_{x=\infty}$$

The boundary conditions at $x = \infty$ are:

$$\sigma_x = -\frac{M}{I}y; \quad \sigma_y = 0 \; ; \quad \tau_{xy} = 0$$

Inserting Equations (21) into the first of Equations (15) along with these boundary conditions gives:

$$-\frac{M}{I}y = 2\left[\sum_1^\infty n A_n (x + iy)^{n-1} + \sum_1^\infty n\bar{A}_n (x - iy)^{n-1}\right]_{x=\infty}$$

This requires that $A_n = 0$ for all values of n except 2. For $n = 2$

$$-\frac{M}{I}y = 2\left[2iA_2 y - 2i\bar{A}_2 y\right]$$

$$A_2 = 1\,\frac{M}{8I}$$

Inserting Equations (21) into the second of Equations (15) gives:

$$\frac{M}{I}y = 2\left[(x - iy)\cdot 2\cdot 1\cdot A_2 + \sum_1^\infty n B_n (x + iy)^{n-1}\right]_{x=\infty}$$

This requires that $B_n = 0$ for all values of n except 2. For $n = 2$

$$\frac{M}{I}y = 2\left[\frac{M}{4I}y + 2iB_2 y\right]$$

$$B_2 = -\,i\,\frac{M}{8I}y = -A_2$$

Therefore, for pure bending, regardless of the shape of the opening, the potential functions are:

$$\Phi(z) = \frac{iM}{8I}y^2 + \sum_1^\infty a_n/z_n$$

$$\Psi(z) = -\frac{iM}{8I}y^2 + \sum_1^\infty b_n/z_n \qquad (22)$$

On the boundary of this opening:

$$\varphi(\lambda) = \frac{iM}{8I}\left(s\lambda + \frac{t}{\lambda} + \frac{R}{\lambda^3}\right)^2 + \sum_{1}^{\infty} \frac{b_n}{\left(s\lambda + \frac{t}{\lambda} + \frac{R}{\lambda^3}\right)^n}$$

$$\bar{\varphi}'\left(\frac{1}{\lambda}\right) = \left[-\frac{iM}{4I}\left(\frac{s}{\lambda} + t\lambda + R\lambda^3\right) - \sum_{1}^{\infty} \frac{n\bar{a}_n}{\left(\frac{s}{\lambda} + t\lambda + R\lambda^3\right)^{n+1}}\right] Z'\left(\frac{1}{\lambda}\right)$$

$$\psi(\lambda) = -\frac{iM}{8I}\left(s\lambda + \frac{t}{\lambda} + \frac{R}{\lambda^3}\right)^2 + \sum_{1}^{\infty} \frac{b_n}{\left(s\lambda + \frac{t}{\lambda} + \frac{R}{\lambda^3}\right)^n}$$

$$\bar{\psi}'\left(\frac{1}{\lambda}\right) = \frac{iM}{8I}\left(\frac{s}{\lambda} + t\lambda + R\lambda^3\right)^2 + \sum_{1}^{\infty} \frac{\bar{b}_n}{\left(\frac{s}{\lambda} + t\lambda + R\lambda^3\right)^n}$$

The boundary condition (20) becomes:

$$\varphi(\lambda) - \frac{s\lambda^4 + t\lambda^2 + R}{\lambda^3}\left[\frac{iM}{4I}\left(\frac{s}{\lambda} + t\lambda + R\lambda^3\right) + \sum_{1}^{\infty} \frac{n\bar{a}_n}{\left(\frac{s}{\lambda} + t\lambda + R\lambda^3\right)^{n+1}}\right]$$

$$+ \frac{iM}{8I}\left(\frac{s}{\lambda} + t\lambda + R\lambda^3\right)^2 + \sum_{1}^{\infty} \frac{\bar{b}_n}{\left(\frac{s}{\lambda} + t\lambda + R\lambda^3\right)^n} = 0 \qquad (23)$$

Expanding and collecting terms:

$$\psi(\lambda) - \frac{iM}{4I}(s^2 + t^2 + R^2 - st) - \frac{iM}{8I}(2st + 2Rt - t^2 - 2Rs)\lambda^2$$

$$- \frac{iM}{8I}(2Rs - 2Rt)\lambda^4 + \frac{iM}{8I}R^2\lambda^6 - \frac{iM}{8I}\left(\frac{2st + 2Rt - s^2}{\lambda^2}\right)$$

$$- \frac{iM}{8I}\frac{2Rs}{\lambda^4} - \sum_{1}^{\infty} \frac{n\bar{a}_n}{\left(\frac{s}{\lambda} + t\lambda + R\lambda^3\right)^{n+1}}\left(\frac{s\lambda^4 + t\lambda^2 + R}{\lambda^3}\right)$$

$$+ \sum_{1}^{\infty} \frac{\bar{b}_n}{\left(\frac{s}{\lambda} + t\lambda + R\lambda^3\right)^n} = 0$$

At $\zeta = 0$, $\varphi(\zeta)$ has the form:

$$\psi(\zeta) = \varphi(\zeta) + \frac{iM}{8I}\left(\frac{2st + 2Rt - s^2}{\zeta^2}\right) + \frac{iM}{8I} \cdot \frac{2Rs}{\zeta^4} + \frac{M\bar{a}_1}{s^2\zeta}$$

From Theorem I:

$$\frac{1}{2\pi i}\int_{\gamma}\frac{\varphi(\lambda)d\lambda}{\lambda-\zeta} = -\frac{iM}{8I}\left(\frac{2st+2Rt-s^2}{\zeta^2}\right) - \frac{iM}{8I}\cdot\frac{2Rs}{\zeta^4} - \frac{R\bar{a}_1}{s^2\zeta}$$

for $|\zeta| > 1$

$$\frac{1}{2\pi i}\int_{\gamma}\frac{\lambda\varphi(\lambda)d\lambda}{\lambda-\zeta} = -\frac{iM}{8I}\left(\frac{2st+2Rt-s^2}{\zeta^2}\right) - \frac{iM}{8I}\cdot\frac{2Rs}{\zeta^4}$$

for $|\zeta| > 1$

At $\zeta = \infty$, $\varphi(\zeta)$ has the form:

$$\varphi(\zeta) = \frac{iM}{8I}s^2\zeta^2 + \sum_{-\infty}^{\infty}\frac{D_K}{\zeta^K}$$

From Theorem II:

$$\frac{1}{2\pi i}\int_{\gamma}\frac{\varphi(\lambda)d\lambda}{\lambda-\zeta} = -\varphi(\zeta) + \frac{iM}{8I}s^2\zeta^2 \qquad \text{for } |\zeta|>1$$

$$\frac{1}{2\pi i}\int_{\gamma}\frac{\lambda\varphi(\lambda)d\lambda}{\lambda-\zeta} = -\zeta\varphi(\zeta) + \frac{iM}{8I}s^2\zeta^3 \qquad \text{for } |\zeta|>1$$

From the first of the expressions derived from each theorem:

$$\varphi(\zeta) = \frac{iM}{8I}\left[s^2\zeta^2\,\frac{2st+2Rt-s^2}{\zeta^2} + \frac{2Rs}{\zeta^4}\right] + \frac{R\bar{a}_1}{s^2\zeta} \qquad (24)$$

From the second of the expressions derived from each theorem:

$$\zeta\varphi(\zeta) = \frac{iM}{8I}\left[s^2\zeta^3\,\frac{2st+2Rt-s^2}{\zeta} + \frac{2Rs}{\zeta^3}\right] \qquad (25)$$

Comparing (24) and (25):

$$\bar{a}_1 = 0$$

Putting $T = t + \frac{Rt}{s} - \frac{1}{2}s$

$$\varphi(\zeta) = \frac{iMs}{4I}\left[\frac{s}{2}\zeta^2 + \frac{T}{\zeta^2} + \frac{R}{\zeta^4}\right] \qquad (26)$$

But the conjugate of Equation (26) is:

$$\bar{\varphi}\left(\frac{1}{\lambda}\right) + \frac{z\left(\frac{1}{\lambda}\right)}{z'(\lambda)}\varphi'(\lambda) + \psi(\lambda) = 0$$

Using Equation (26), this becomes:

$$-\frac{iMs}{4I}\left[\frac{s}{2\lambda^2} + T\lambda^2 + R\lambda^4\right] + \frac{iMs}{4I}\left(s\lambda - \frac{2T}{\lambda^3} - \frac{4R}{\lambda^5}\right)\frac{\left(\frac{s}{\lambda} + t\lambda + R\lambda^3\right)}{\left(s - \frac{t}{\lambda^2} - \frac{3R}{\lambda^4}\right)}$$

$$+ \psi(\lambda) = 0$$

$$\psi(\lambda) = \frac{iMs}{4I}\left[\frac{s}{2\lambda^2} + T\lambda^2 + R\lambda^4 - \frac{s\lambda^4 - 2T - \frac{4R}{\lambda^2}}{s\lambda^4 - t\lambda^2 - 3R}\left(s + t\lambda^2 + R\lambda^4\right)\right]$$

At $\zeta = 0$, $\psi(\zeta)$ has the form:

$$\psi(\zeta) = \frac{iMs}{4I}\left(\frac{s}{2\zeta^2}\right) + g(\zeta)$$

From Theorem I:

$$\frac{1}{2\pi i}\int_{\Upsilon}\frac{\psi(\lambda)d\lambda}{\lambda - \zeta} = -\frac{iMs}{4I}\left(\frac{s}{2\zeta^2}\right) \qquad \text{for } |\zeta| > 1$$

At $\zeta = \infty$, $\psi(\zeta)$ has the form:

$$\psi(\zeta) = \frac{iMs}{4I}\left[T\zeta^2 + R\zeta^4 - \frac{s\zeta^4 - 2T - \frac{4R}{\zeta^2}}{s\zeta^4 - t\zeta^2 - 3R}\left(s + t\zeta^2 + R\zeta^4\right)\right]$$

From Theorem II:

$$\frac{1}{2\pi i}\int_{\Upsilon}\frac{\psi(\lambda)d\lambda}{\lambda - \zeta} = -\psi(\zeta) + \frac{iMs}{4I}\left[T\zeta^2 + R\zeta^4 - \frac{s\zeta^4 - 2T - \frac{4R}{\zeta^2}}{s\zeta^4 - t\zeta^2 - 3R}\left(s + t\zeta^2 + R\zeta^4\right)\right] \qquad \text{for } |\zeta| > 1$$

Therefore:

$$\varphi(\zeta) = \frac{iMs}{4I}\left[-\frac{s}{2\zeta^2} + T\zeta^2 + R\zeta^4 - \frac{s\zeta^4 - 2 - \frac{4R}{\zeta^2}}{s\zeta^4 - t\zeta^2 - 3R}(s + t\zeta^2 + R\zeta^4)\right]$$

(27)

Using the first of Equations (17) and noting that at a free boundary $\alpha = 0$, $\sigma_\alpha = 0$

$$(\sigma_\beta)_{\alpha=0} = 2\left[\Phi'(z) + \bar{\Phi}'(z)\right]_{\alpha=0} = 2\left[\frac{\varphi'(\lambda)}{z'(\lambda)} \quad \frac{\bar{\varphi}'(\frac{1}{\lambda})}{z'(\frac{1}{\lambda})}\right]$$

But

$$\varphi(\lambda) = \frac{iMs}{4I}\left[\frac{s\lambda^2}{2} + \frac{T}{\lambda^2} + \frac{R}{\lambda^4}\right] \quad \text{and} \quad \bar{\varphi}(\frac{1}{\lambda}) = -\frac{iMs}{4I}\left[-\frac{s}{2\lambda^2} + T\lambda^2 + R\lambda^4\right]$$

$$\varphi'(\lambda) = \frac{iMs}{4I}\left[s\lambda - \frac{2T}{\lambda^3} - \frac{4R}{\lambda^5}\right] \quad \text{and} \quad \bar{\varphi}'(\frac{1}{\lambda}) = -\frac{iMs}{4I}\left[\frac{s}{\lambda} - 2T\lambda^3 - 4R\lambda^5\right]$$

$$z'(\lambda) = s - \frac{t}{\lambda^2} - \frac{3R}{\lambda^4} \quad \text{and} \quad \bar{z}'(\frac{1}{\lambda}) = s - t\lambda^2 - 3R\lambda^4$$

Thus:

$$(\sigma_\beta)_{\alpha=0} = 2\left[\frac{iMs}{4I} \cdot \frac{s\lambda - \frac{2T}{\lambda^3} - \frac{4R}{\lambda^5}}{s - \frac{t}{\lambda^2} - \frac{3R}{\lambda^4}} - \frac{iMs}{4I} \cdot \frac{\frac{s}{\lambda} - 2T\lambda^3 - 4R\lambda^5}{s - t\lambda^2 - 3R\lambda^4}\right]$$

$$(\sigma_\beta)_{\alpha=0} = -\frac{Ms}{I}\left[\frac{(s^2 + 6Rt - 2tT - 12R^2)\sin\beta - (2Rt - st + s^2)\sin 3\beta + Rs\sin 5\beta}{(s^2 + t^2 + 9R^2) + (6Rt - 2st)\cos 2\beta - 6Rs\cos 4\beta}\right]$$

(28)

$(\sigma_\beta)_{\alpha=0}$ is a maximum when $\beta = 90^\circ$.

Therefore:

$$SCF = \frac{(\sigma_\beta)_{\alpha=0}}{-\frac{My_0}{I}} = \frac{s}{y_0}\left[\frac{2s^2 - 3Rs - 12R^2 + 2t(4R - t)(1 + \frac{R}{s})}{(s + t - 3R)^2}\right] \qquad (28a)$$

If we now substitute Equations (1), (9), (26), (27), and (11) into Equation (14), integrate and combine terms, we get the Airy stress function:

$$F(\alpha,\beta) = \frac{Ms}{4I}\left\{\left[(s^2+3t-2Rt+3R^2)e^{\alpha} + (3RT - \frac{s^2}{2} - 2Tt - 4R^2)e^{-\alpha}\right.\right.$$

$$\left. - \frac{s^2}{2}e^{+3\alpha} + Rte^{-3\alpha} - RTe^{-5\alpha} + R^2e^{-7\alpha}\right] \sin\beta$$

$$+ \left[\left(\frac{st + Rt - sT}{3}\right)e^{3\alpha} + \left(\frac{st}{6} - \frac{2sT}{3} - \frac{4Rt}{3}\right)e^{-3\alpha} + sTe^{-\alpha}\right.$$

$$\left. \left. - \frac{st}{4}e^{\alpha} + Rte^{-5\alpha}\right] \sin 3\beta + \left[Rse^{-3\alpha} - \frac{Rs}{2}e^{-\alpha} - \frac{Rs}{2}e^{-5\alpha}\right] \sin 5\beta \right\}$$

(29)

Evaluation of Parameters

It is necessary to determine the values of R, s, and t that will ensure that the mapping function ( ) will suit the actual opening when $\alpha = 0$. Several conditions may be imposed on (10a) in order to determine R, s, and t such as:

(a) $s + t + R = \frac{1}{2}$ horizontal dimension $= \frac{1}{2}a$

(b) $s - t + R = \frac{1}{2}$ vertical dimension $= \frac{1}{2}b$

(c) Area of opening $= (a - b)b + \frac{1}{4}b^2\pi = \int y\,dx$

(d) Radius of curvature at end $= \frac{1}{2}b$

Equations associating the desired variables with the geometric properties of the opening must now be developed to provide a systematic procedure for evaluation. To simplify this problem we introduce the Greenspan notation:

$$\begin{aligned} \tfrac{1}{2}(P + Q) &= s \\ \tfrac{1}{2}(P - Q) &= t \end{aligned} \qquad (30)$$

Or:

$$\begin{aligned} s + t &= P \\ s - t &= Q \end{aligned} \qquad (30a)$$

Then, Equations (10a) become:

$$\begin{aligned} x &= P\cos\beta + R\cos 3\beta \\ y &= Q\sin\beta - R\sin 3\beta \end{aligned} \qquad (10b)$$

Imposing the condition of equal areas, we obtain:

$$4\int_0^{\frac{1}{2}a} y\,dx = (a - b)b + \tfrac{1}{4}b^2\pi \quad \text{for } a > b \qquad (31)$$

Substituting (10b) into (31), integrating, and simplifying gives:

$$\pi\ (P^2 - 3R^2) = (a - b)b + \tfrac{1}{2}b^2\pi \qquad (32)$$

Reference to any text on differential calculus shows that the radius of curvature at any point is given by the expression:

$$\text{Radius} = \frac{(1 + y'^2)^{3/2}}{y''} \qquad (33)$$

Now: $y' = \frac{dy}{dx} = \frac{dy}{d\beta} \cdot \frac{d\beta}{dx}$ and $y'' = \frac{dy'}{dx} = \frac{dy'}{d\beta} \cdot \frac{d\beta}{dx}$

But, $\frac{dy}{d\beta} = Q \cos\beta - 3R \cos 3\beta$

and $\frac{d\beta}{dx} = -\frac{1}{P \sin\beta + 3R \sin 3\beta}$

Hence: $y' = -\frac{Q \cos\beta - 3R \cos 3\beta}{P \sin\beta + 3R \sin 3\beta} \qquad (34)$

and $y'' = +\frac{-PQ + 27R^2 - 3R(P + Q)\cos 4\beta + 6R(P-Q)\cos 2\beta}{(P \sin\beta + 3R \sin 3\beta)^2}$

(35)

Substituting (34) and (35) into (33) and simplifying gives:

$$\text{Radius} = \frac{\frac{1}{2}(P^2+Q^2)+(-\frac{1}{2}P^2+3PR-3QR+\frac{1}{2}Q^2)\cos 2\beta - 3R(P+Q)\cos 4\beta + 9R^2}{-PQ+27R^2-3R(P+Q)\cos 4\beta+6R(P-Q)\cos 2\beta}$$

Now $\beta = 0$ for the longitudinal end of the opening.

Therefore:

$$\text{Radius} = \frac{(\quad - 3R)^2}{P + 9R} = \tfrac{1}{2}b \qquad (37)$$

The remaining two equations are simply:

$$P + R = \tfrac{1}{2}a \qquad (38)$$

$$Q + R = \tfrac{1}{2}b \qquad (39)$$

Considering only Equations (32), (37), (38), and (39) as a system of equations for the determination of P, Q, and R, we now choose b = 2 and involve the ratio of length to depth of opening, a/b . The system of equations become:

$$
\begin{aligned}
&P \neq R = a/b \\
&Q \neq R = 1 \\
&PQ - 3R^2 = \frac{4}{\pi}(a/b - 1) \neq 1 \\
&\frac{(Q - 3R)^2}{P \neq 9R} = 1
\end{aligned}
\tag{40}
$$

Any system of more equations than there are unknowns is indeterminate. Therefore, the four possible combinations of (40) taken three at a time were solved for P, Q, and R for the particular case of a/b = 2. This particular case was chosen since it had been used by Greenspan [7] as an illustration and a ready comparison was available. The outline of the opening as defined by these four solutions are plotted in Fig. XVI and compared with the actual opening for which the fit was desired.

Because the ratio of depth of opening to depth of beam is an important criterion in the determination of the stress concentration factor, the depth of opening seemed the most logical first choice to be held constant. Next in importance as governing variable was the length of opening. To complete the system of equations for solution for P, Q, and R either the radius of curvature at the longitudinal end or the area must be chosen. A comparison of the fit showed that either

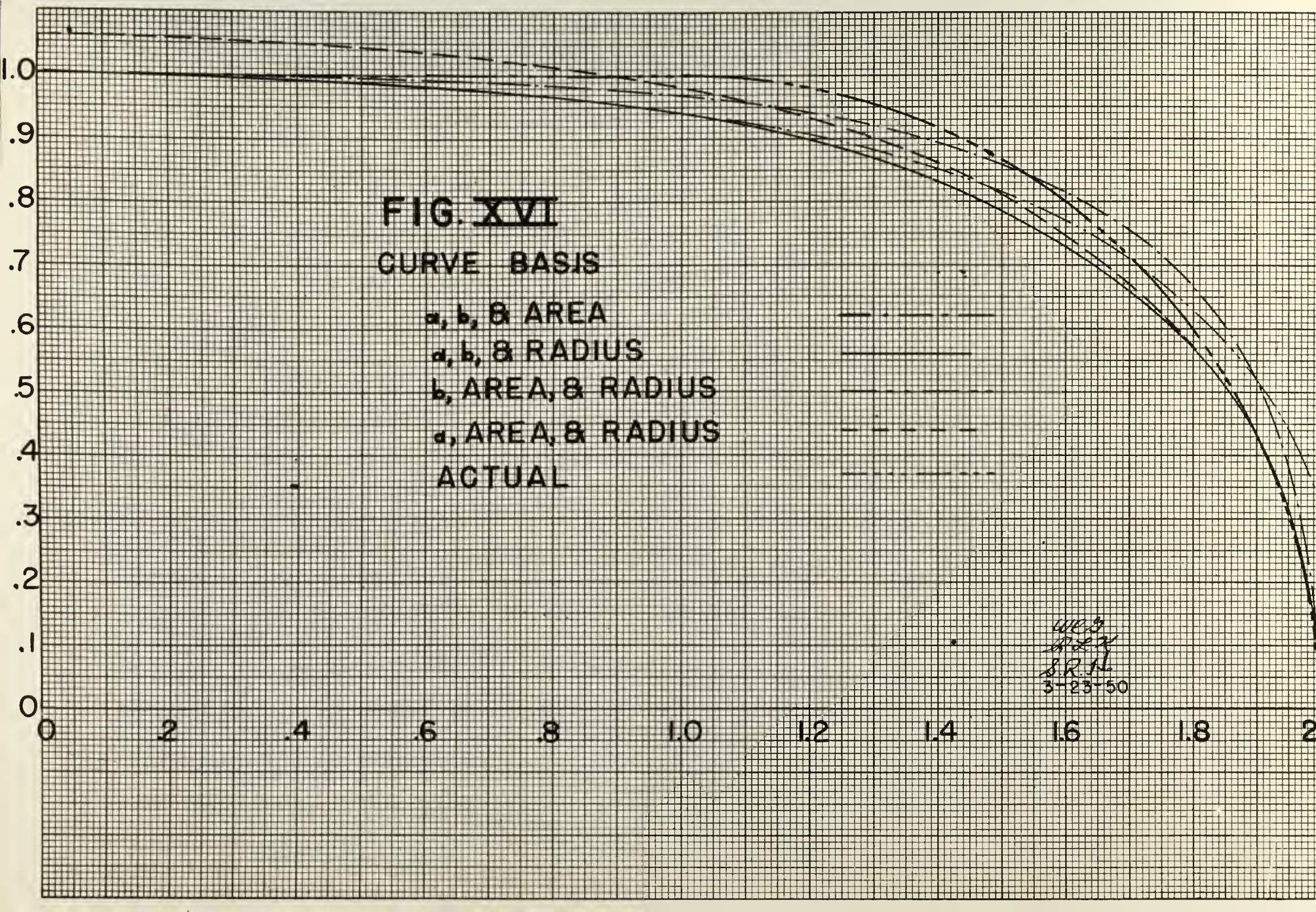
1.0
.9
.8
.7
.6
.5
.4
.3
.2
.1
0
0
.2
.4
.6
.8
1.0
1.2
1.4
1.6
1.8
2
FIG. XVI
CURVE BASIS
a, b, & AREA
a, b, & RADIUS
b, AREA, & RADIUS
a, AREA, & RADIUS
ACTUAL
W.C.B.
A.E.Y.
S.R.M.
3-23-50

would be satisfactory, and a comparison of the two values of stress concentration factor examined with Greenspan's value as the yardstick showed that either would be satisfactory. A good case could be made for holding the end radius of curvature equal to the half height of opening since this system gave values of stress concentration factor that were slightly high - pessimistic. When plotted on a curve similar to Fig. III, however, the closeness of fit of values calculated by holding the area constant was slightly superior to those values calculated by holding the end radius of curvature equal to the half height of opening. The ease of calculating the values of P, Q, and R when holding the area constant was a further consideration.

Consequently a system of equations consisting of the first three of Equations (40) was chosen:

$$P = a/b - R$$

$$Q = 1 - P \qquad (40)$$

$$PQ - 3R^2 = \frac{4}{\pi}(a/b - 1) \neq 1$$

From which:

$$R = -\tfrac{1}{3}(a/b \neq 1) \neq \tfrac{1}{3}\sqrt{(a/b \neq 1)^2 - 3(4/\pi - 1)(a/b - 1)} \qquad (40a)$$

These values of P, Q, and R are plotted versus a/b in Fig. XVII.

This should not be construed to mean that these values are precise; they are merely the best choice that the authors could make with existing information. Some other geometric property, such as the peripheral length, may warrant consideration.

FIG. XVII

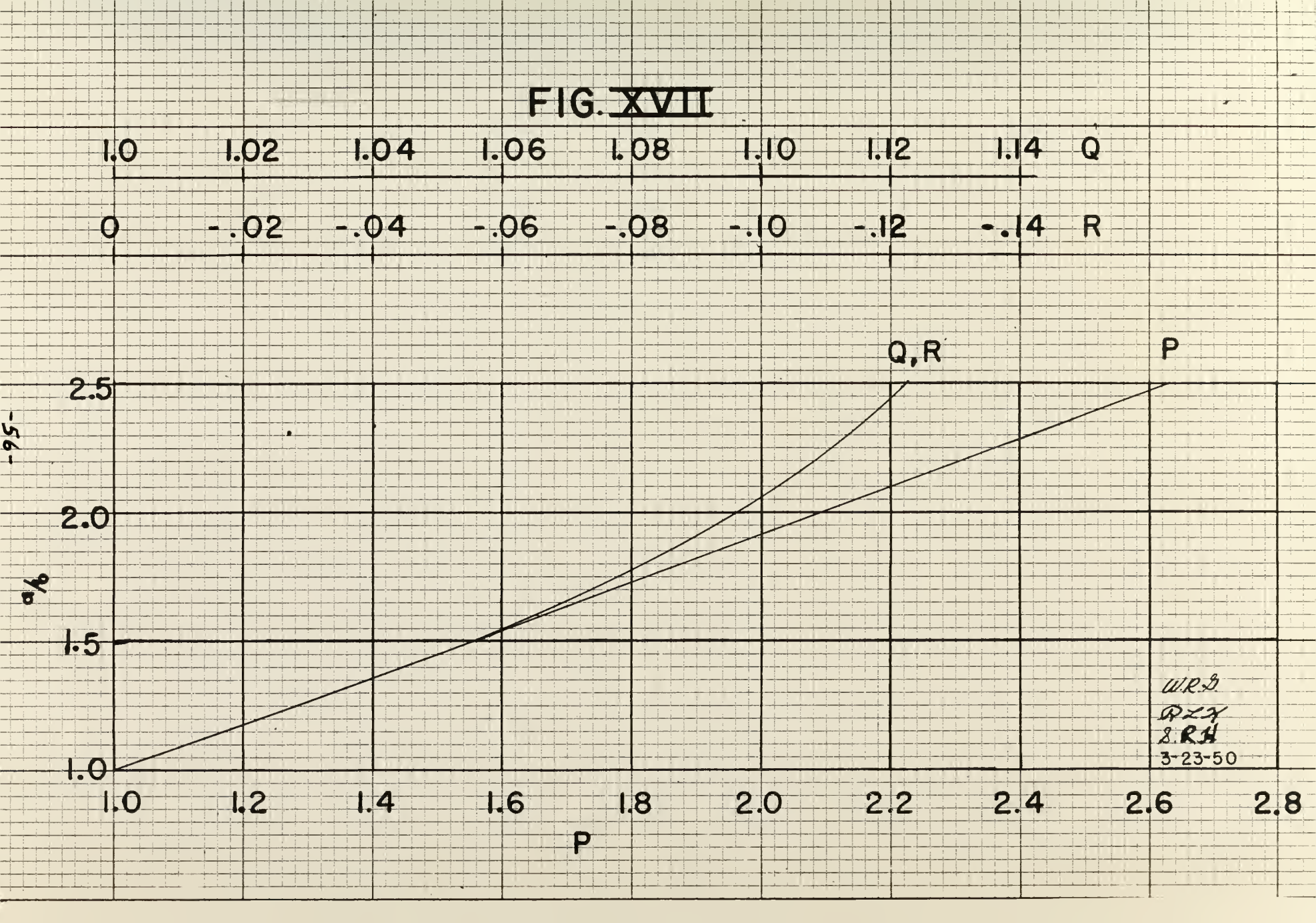
1.0
1.02
1.04
1.06
1.08
1.10
1.12
1.14
Q
0
-.02
-.04
-.06
-.08
-.10
-.12
-.14
R
Q, R
P
2.5
2.0
1.5
1.0
a/b
1.0
1.2
1.4
1.6
1.8
2.0
2.2
2.4
2.6
2.8
P
W.R.S.
R.L.Y.
S.R.H.
3-23-50

APPENDIX E

APPENDIX E

Bibliography

(1) Kirsch, G.: "Die Theorie Der Elastizitätund Die Bedürfnisse Der Festigkeitslehre", Zeitschrift Des Vereines Deutscher Ingenieure, Vol. 42, 1898.

(2) Tuzi, Z.: "Effect of a Circular Hole on the Stress Distribution of a Beam Under Uniform Bending Moment", Scientific Papers of the Tokyo Institute of Physical and Chemical Research, Vol. 9, Aug. 20, 1928, pp. 65 - 89.

(3) Howland, R. C. J., and Stevenson, A. C.: "Biharmonic Analysis in a Perforated Strip", Philosophic Transactions of the Royal Society of London, Series A, vol. 232, 1933, pp. 155 - 222.

(4) Wolf, K.: "Beiträge zur ebenen Elastizitätstheorie", Zeitschrift fur technische Physik, vol. 2, no. 8, 1921, p. 209, and vol. 3, no. 5, 1922, pp. 160 - 166.

(5) Neuber, H.: "Theory of Notch Stresses", David Taylor Model Basin, Translation No. 74, by F. A. Raven and J. S. Brock, Nov., 1945 (Distributed by J. W. Edwards, Ann Arbor, Mich.)

(6) Inglis, C. E.: "Stresses in a Plate Due to the Presence of Cracks and Sharp Corners", Transactions of the Institution of Naval Architects, vol. 55, London 1913, pp. 219 - 242.

(7) Greenspan, M.: "Effect of a Small Hole on the Stresses in a Uniformly Loaded Plate", Quarterly Applied Mathematics, vol. 2, 1944, pp. 60 - 71.

(8) Joseph, J. A. and Brock, J. S.: "The Stresses Around a Small Opening in a Beam Subjected to Pure Bending", Preprint of Paper No. 50 - APM-3 for presentation at the Conference of the Applied Mechanics Division, Purdue University, Lafayette, Ind., June 22 - 24, 1950, of the American Society of Mechanical Engineers.

(9) Timoshenko, S.: "Theory of Elasticity", McGraw-Hill Book Co., Inc., New York, 1934.

(10) Coker, E. G. and Filon, L. N. G.: "A Treatise on Photoelasticity", Cambridge University Press, London, 1931.

(11) Sokolnikoff, I. S.: "Mathematical Theory of Elasticity", (mimeographed lecture notes), Brown University, Providence, Rhode Island, 1941.

DATE DUE			